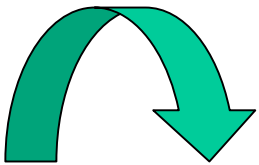


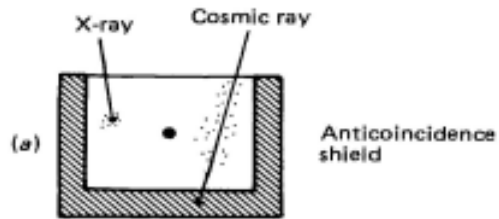
What to measure?

- X-ray emission carries various information - quantify:
 - the position in the sky
 - the time of arrival
 - the energies of the X-rays
 - the brightness of the source (ratio of events over exposure time)
 - [polarization]



- Detectors for non-focusing telescopes
- X-ray focusing optics
- X-ray detectors
- X-ray spectroscopy

Non-focusing X-ray detectors



- to avoid detection of cosmic rays
- shield works as second “detector”
- CR: signal in both devices
- X-rays: signal only in detector

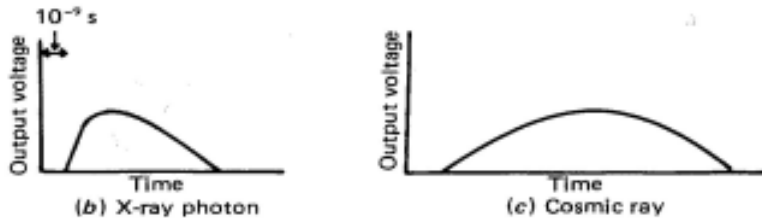
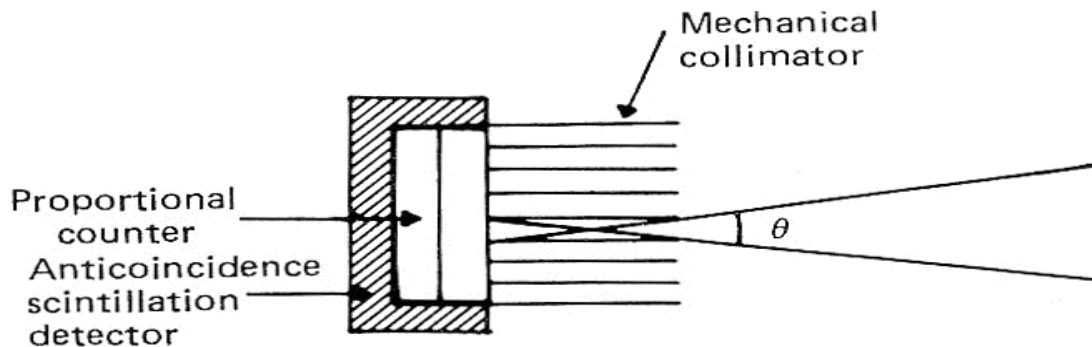


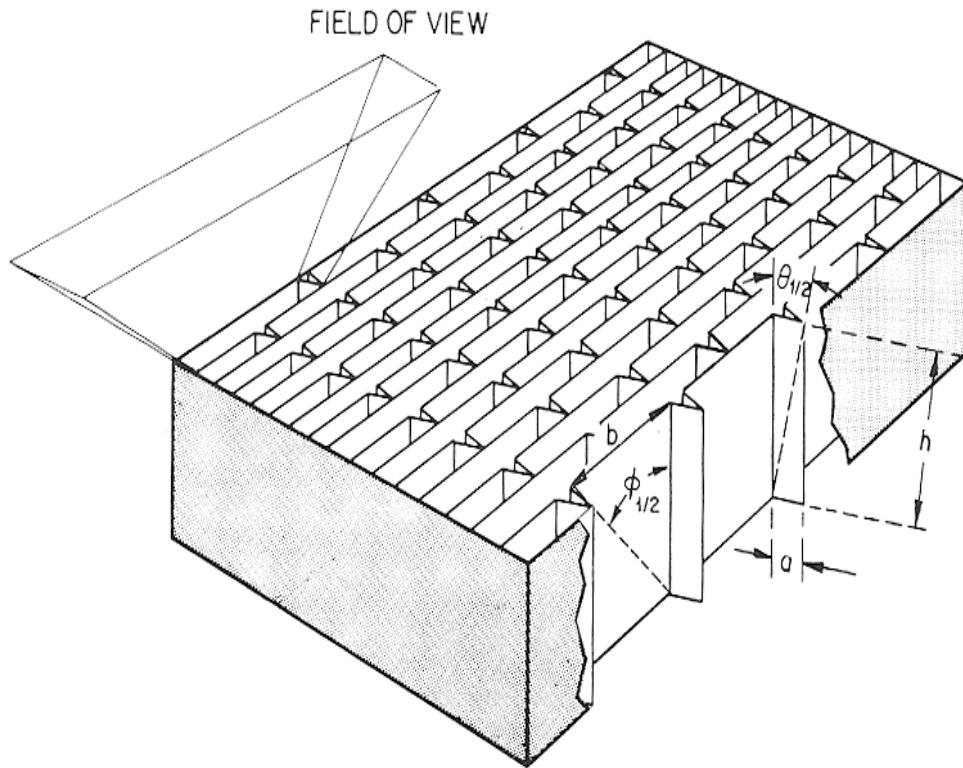
Figure 7.8. Diagrams illustrating the principles of rise-time or pulse-shape discrimination between X-rays and cosmic rays.

➔ Distinction possible



- to avoid light from unwanted directions
- equipped with metallic tubes

Collimator: Example construction

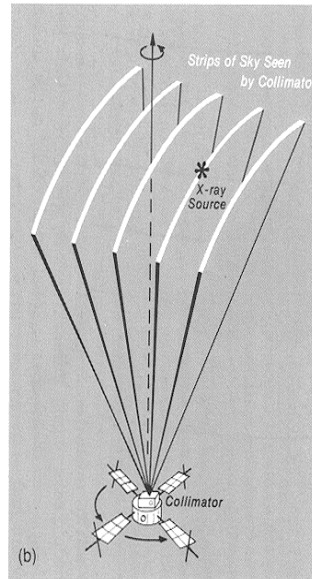
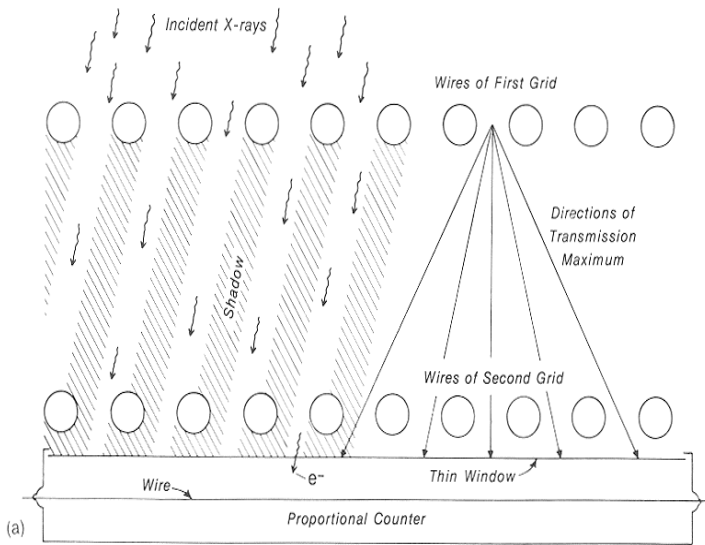


- very high-Z material
- walls extremely thin
➔ max. aperture
- but thick enough to stop X-rays of the highest energies

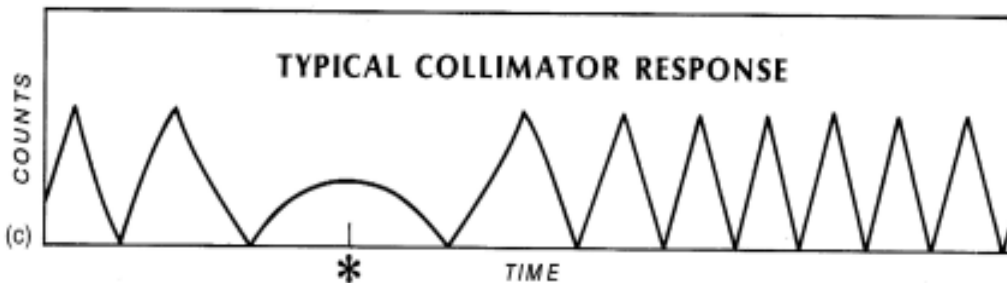
- usage for very long time possible
- cheap

Fig. 2.16. A slat collimator, comprised of rectangular tubes of height h and cross section $a \times b$. X-rays which strike the tubes cannot reach the detector. The response pattern within the field of view has a triangular shape in each of the two orthogonal directions. The half-transmission angles are determined simply by the geometry: $\tan \theta_{1/2} = a/h$; $\tan \phi_{1/2} = b/h$.

Rotation Modulation Collimator



- spinning satellite
 - ➔ rotating collimator
 - ➔ spinning transmission bands on the sky
- proportional counter behind collimator
- observation: count rate vs. time
- modulation of the count rate depends on the position of the overall FOV
 - ➔ **locating X-ray source**
- drawback: **source confusion**



Wolter Optics

1960

1951

Hans Wolter's discovery of a mirror configuration using reflective optics (for developing an X-ray microscope)

Riccardo Giacconi & Bruno Rossi construction of „analogous“ set of optics (not subject to the limitations of fabrication of microscopes)

H. Wolter, Ann. der Physik, 1952, NY 10, 94

R. Giacconi & B. Rossi, JGR, 1960, 65, 773

Annalen der Physik, 6. Folge, Band 10, 1952

Spiegelsysteme streifenden Einfalls als abbildende Optiken für Röntgenstrahlen¹⁾

Von Hans Wolter

(Mit 15 Abbildungen)

Inhaltsübersicht

Als Optiken zur Röntgenstrahlmikroskopie eignen sich Systeme von totalreflektierenden Spiegeln, die bei Befang der sphärischen Aberration für einen Achsenpunkt zugleich die Abbenecke-Strauchbedingung bis zu Aperturen 0,05 befriedigend erfüllen. Für die Lebensdauererwartung längsdauer Objekte erzielbar sind Wellenlängen von 24 Å, die im Wasser wenig, aber in kohlenstoffhaltigen oder stickstoffhaltigen Stoffen stark absorbiert werden. Mit diesen weichen Strahlen ist eine Steigerung des Auflösungsvermögens gegenüber dem Lichtmikroskop um mindestens eine Größenordnung unter Verwendung der hier beschriebenen Optiken zu erwarten.

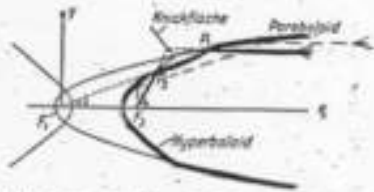


Abb. 6. Paraboloid und Hyperboloid in konfokaler Lage als Spiegelsystem für streifenden Einfall

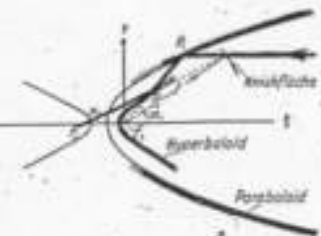


Abb. 15. Spiegelsystem 2. Art

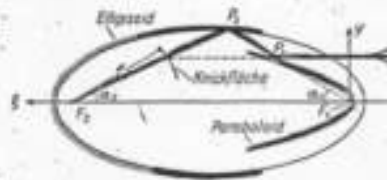
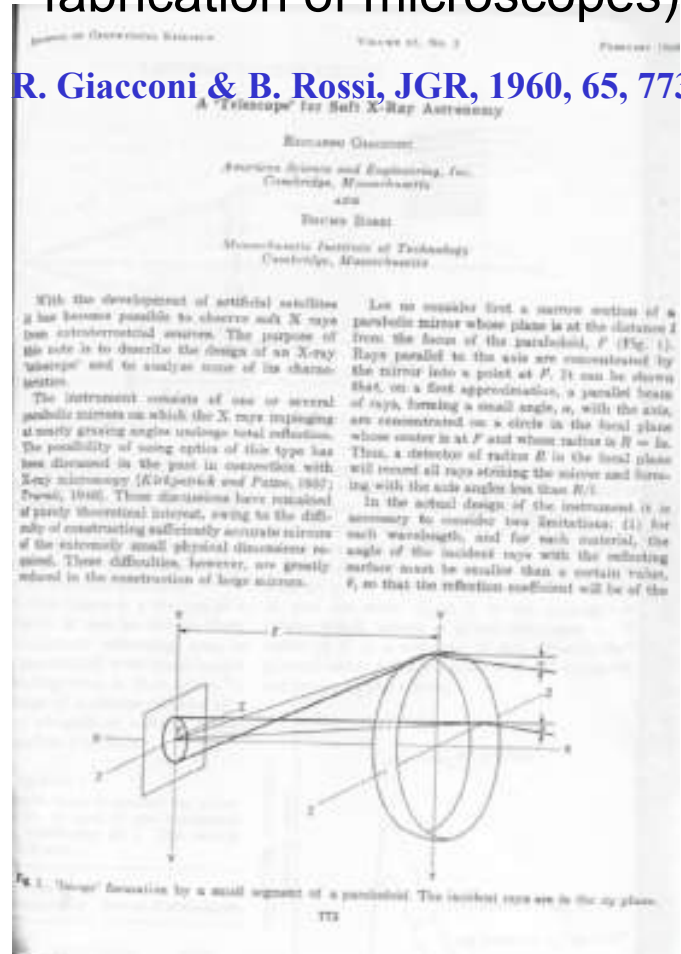


Abb. 16. Spiegelsystem 3. Art



The Nobel Prize in Physics 2002



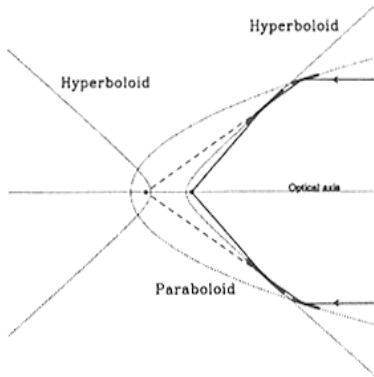
Riccardo Giacconi



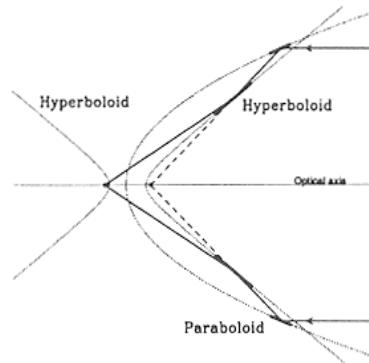
„ for pioneering contributions to astrophysics, which have led to the discovery of cosmic X-ray sources “

Types of Wolter telescopes

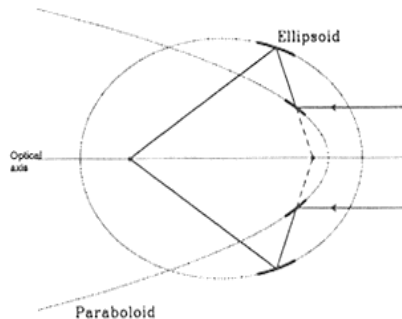
Wolter type I



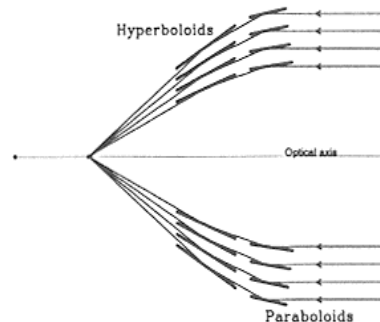
Wolter type II



Wolter type III

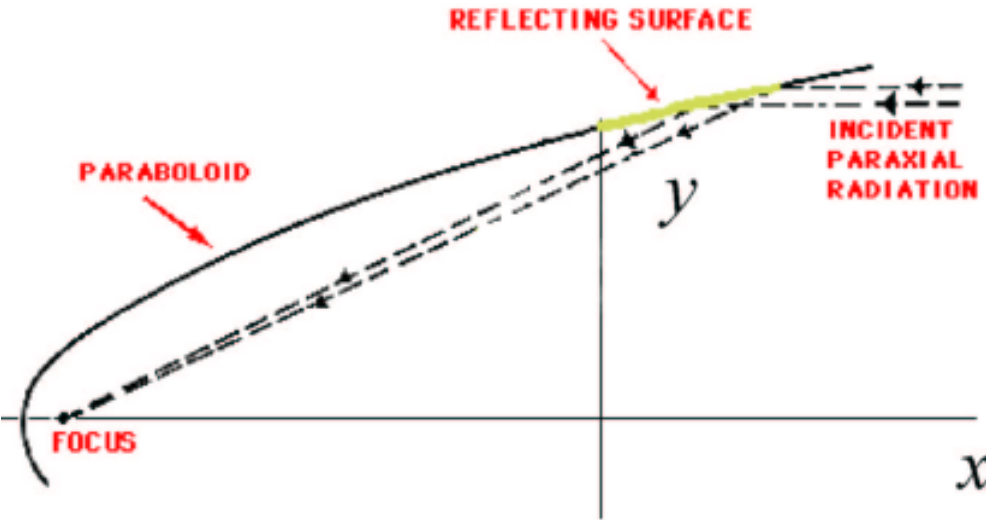


Co-axial Wolter type I



- solution to the X-ray imaging
 - ➔ Wolter type I, II, and III telescopes
- combination of a paraboloid and a hyperboloid/ellipsoid mirror
- mounted confocally and coaxially
- the type I and II telescopes can be built very compact (example: UV telescope on ROSAT)
- the type II telescope resembles the optical Cassegrain system,
- the type III is even more compact, but so far it has never been used

Parabolic X-ray mirror

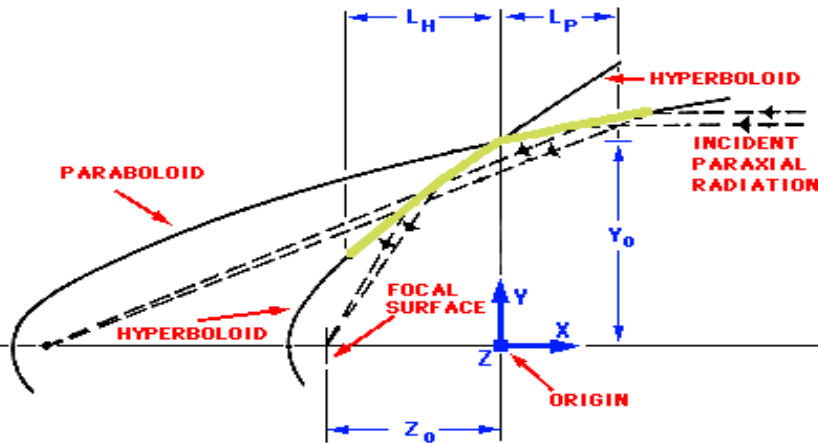


$$y^2 = 2 \cdot p \cdot x$$

$$p = 2 \cdot \text{dist}(\text{focus} - \text{vertex})$$

- known as Wolter type 0 telescope
- perfect on-axis focusing
- BUT: off-axis images suffer extremely from the Coma defect

Wolter type I telescopes (I)



- minimal focal length F for a given aperture Y_0 with

$$F = Y_0 / \tan(4\theta)$$

Y_0 = aperture radius

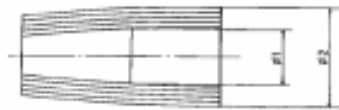
θ = on-axis incidence angle



$$S_v = \frac{\pi \phi_2^2}{4}$$



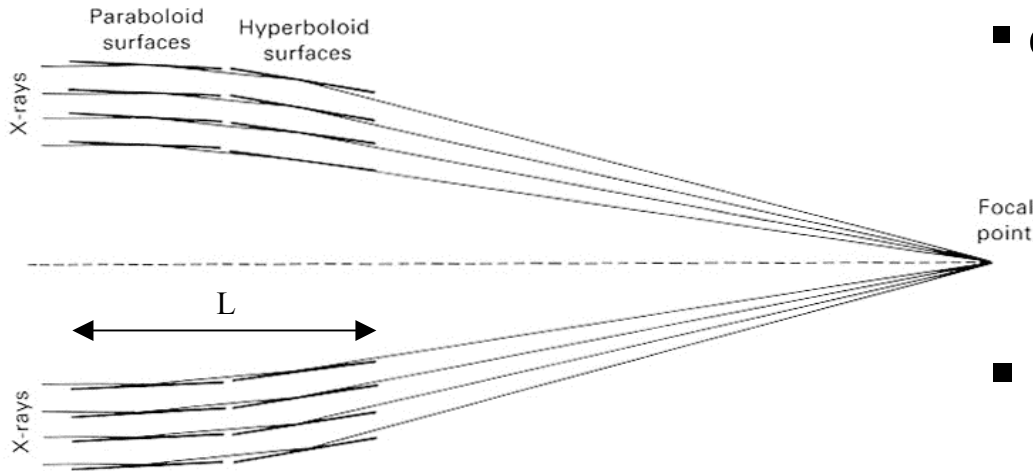
$$S_1 = \frac{\pi (\phi_2 - \phi_1)^2}{4}$$



$$S_x = \frac{\pi (\phi_2 - \phi_1)^2}{4}$$

- geometric area (per shell) rather small because
 - just one ring
 - central X-rays won't be reflected \rightarrow loss
- solution: nesting many confocal mirror shells !!

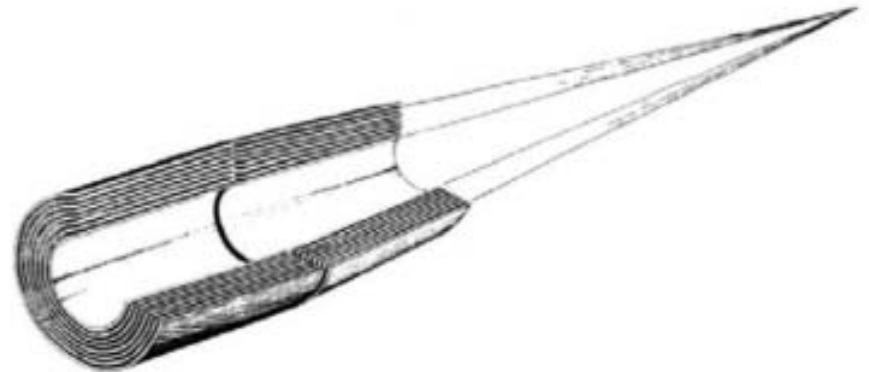
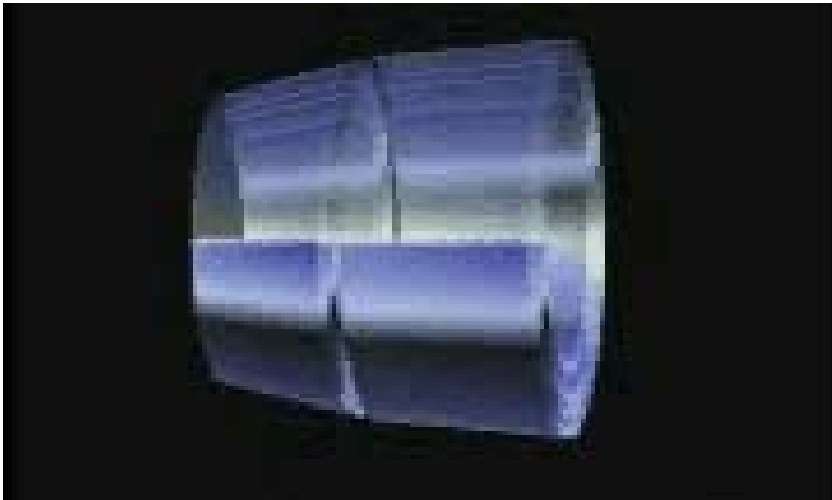
Wolter type I telescopes (II)



- effective area A_{eff} (per shell) is given by

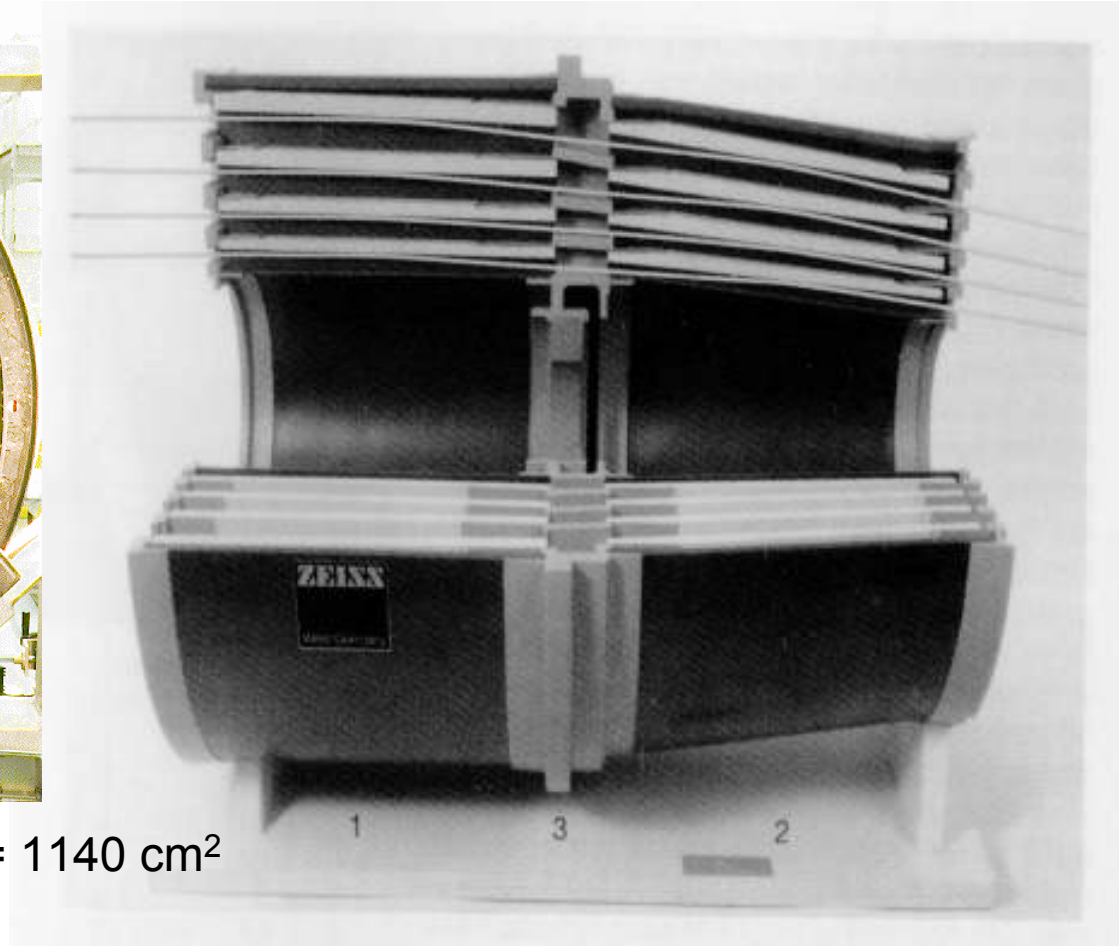
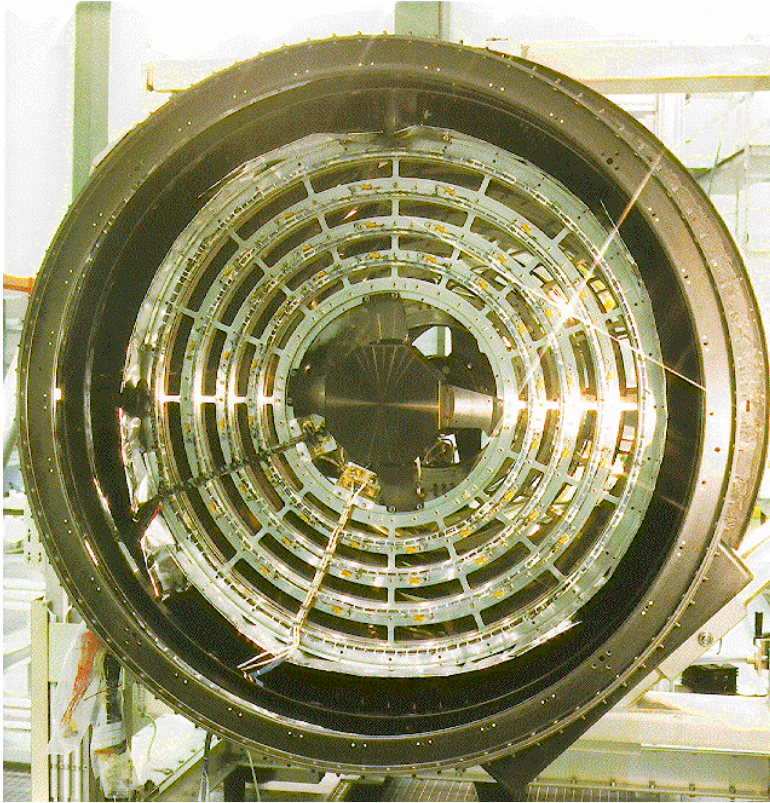
$$A_{\text{eff}} = 8\pi \cdot F \cdot L \cdot \theta^2 \cdot \text{Refl.}^2$$

- solution: nesting many confocal mirror shells can maximise the effective (collecting) area !!



Example: The ROSAT mirrors

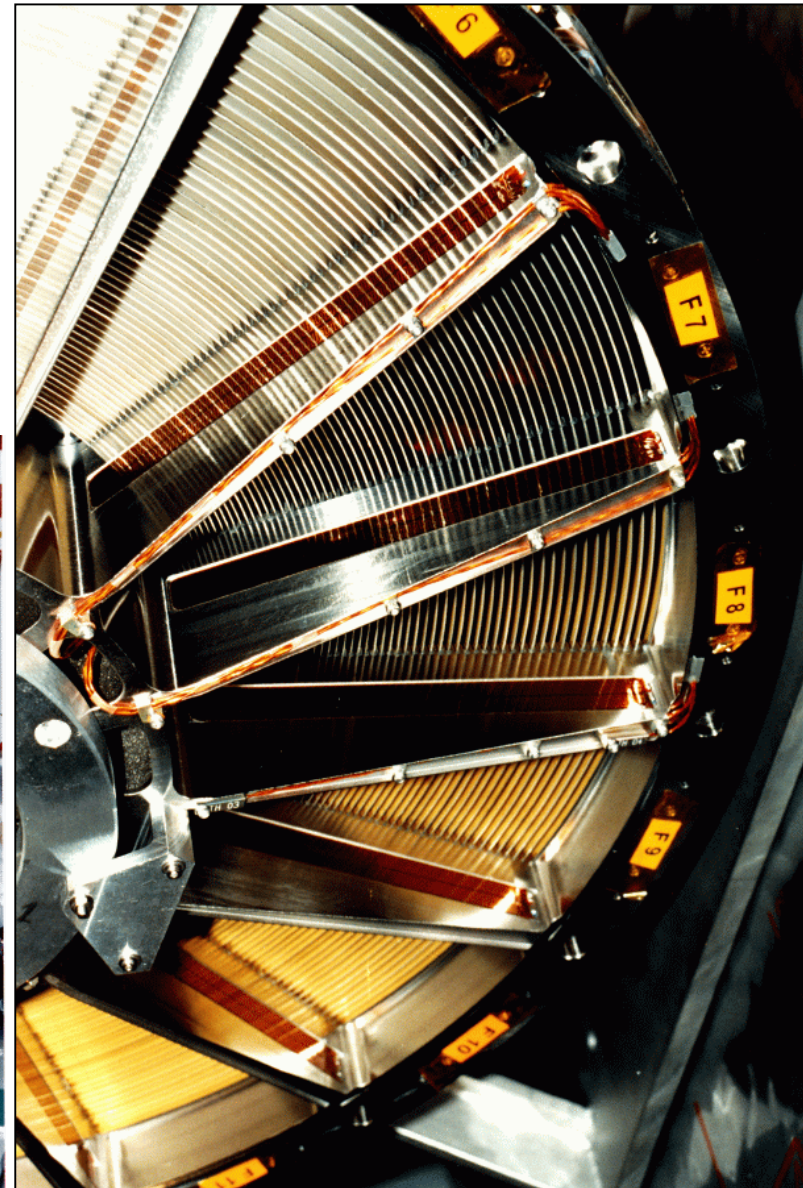
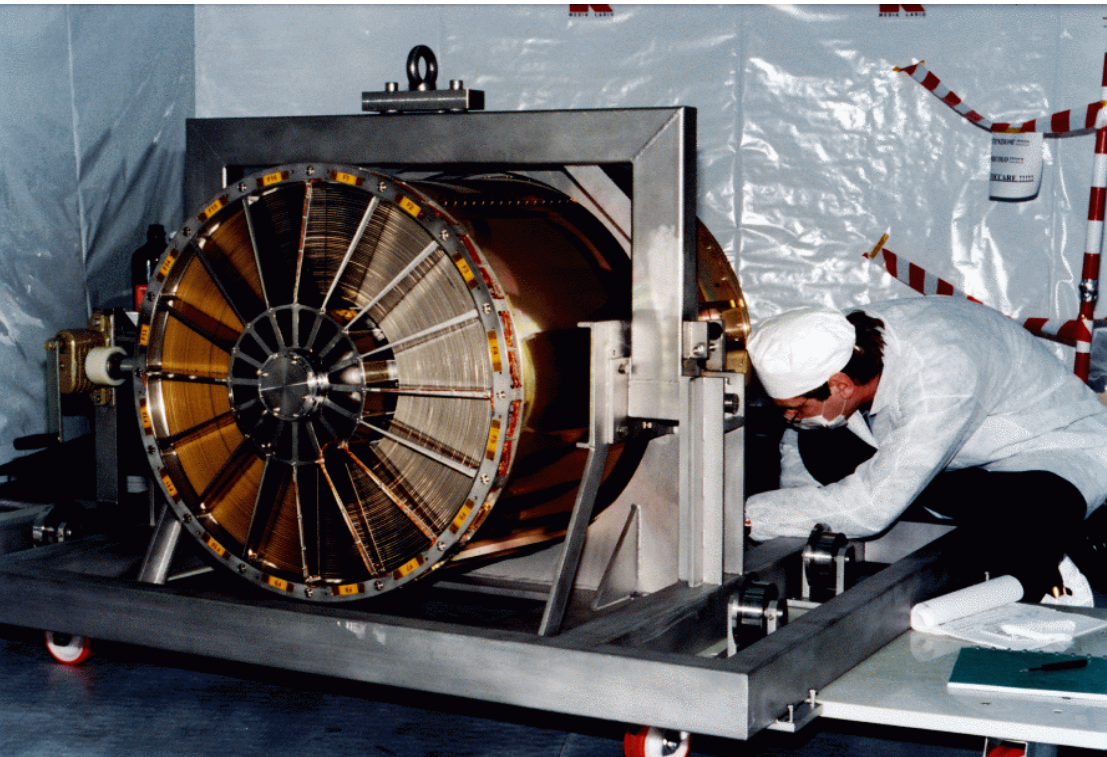
83 cm



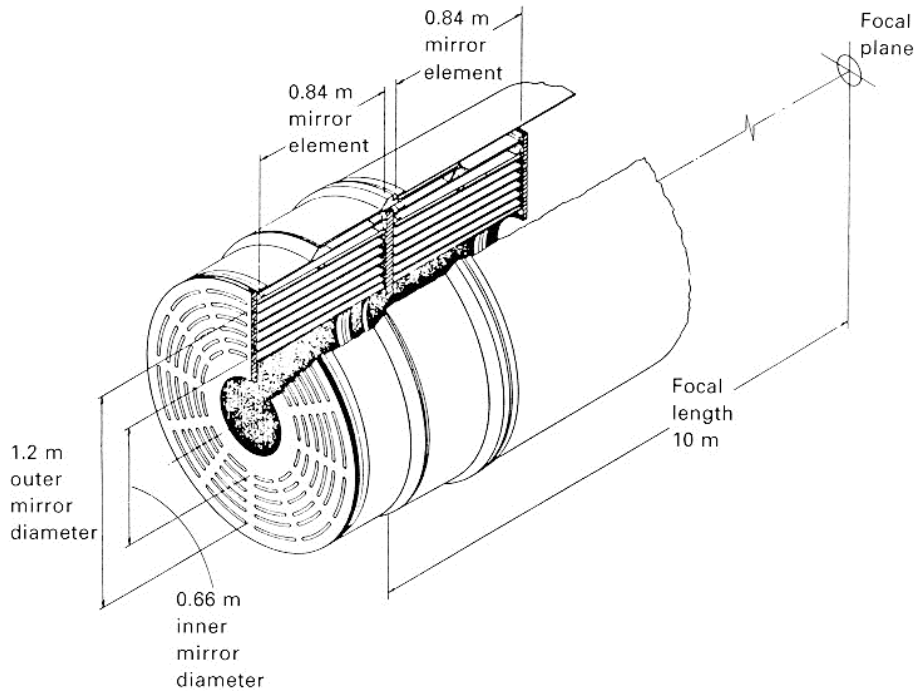
- black slots: total collecting area = 1140 cm²
- focal length = 240 cm

Example: The XMM-Newton mirrors

- segmented thin mirrors
- mirror material: Nickel – coating with Au
- 3 moduls with 58(!) shells/module
- shell thickness: 0.5 mm and 1 mm (very close!)
- focal length = 750 cm, max. diameter = 70 cm
- effective Area @ 1 keV = 1475 cm² /module



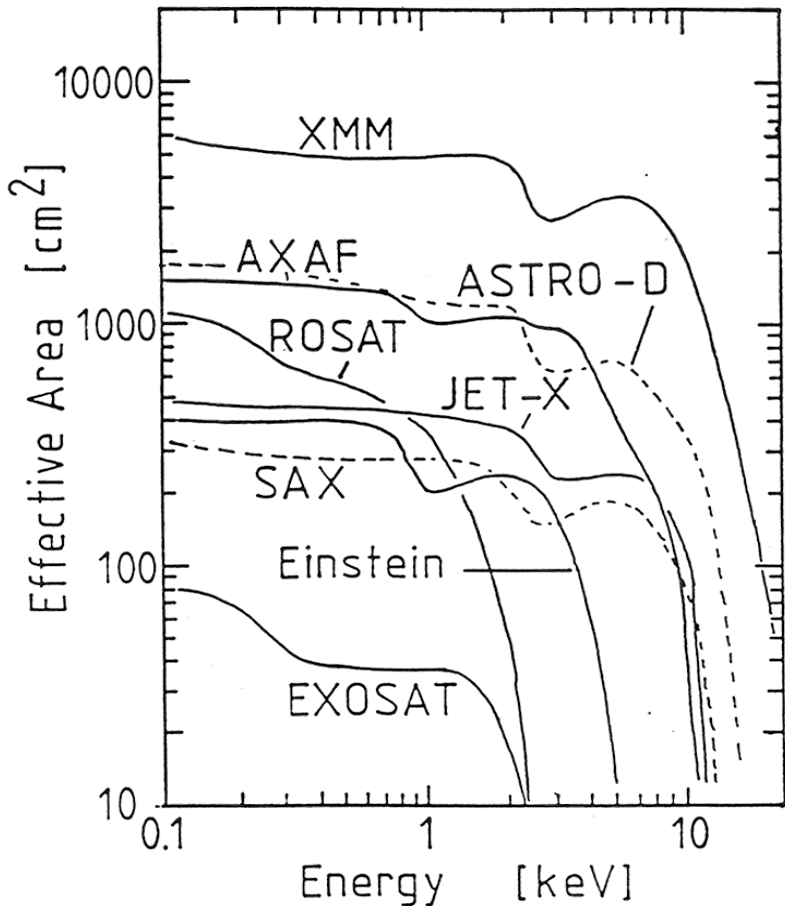
Example: The Chandra Mirrors



- full thick shell mirrors – coating with Ir
- extremely high angular resolution of $1.5''$
- shell's thickness: $\sim 2 - 3$ cm
- made of Zerodur
(= glass with an expansion coefficient = 0)



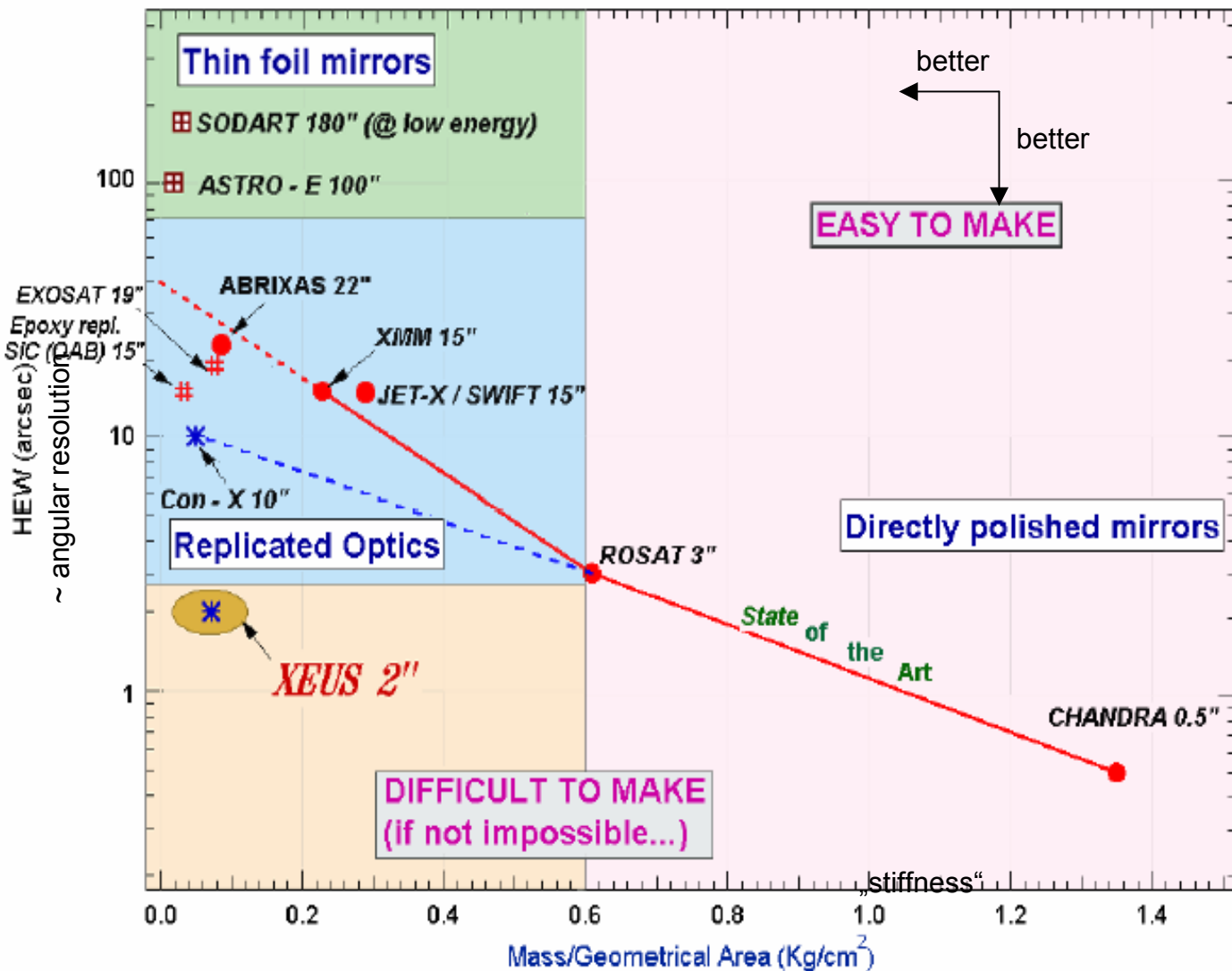
Effective Area



Comparison of effective areas of various X-ray mirrors

- effective Area
= total geometric Area * reflectance
- XMM-Newton: 5 * Chandra
- ~ 2.2 keV:
gold edge (of reflectivity) clearly visible
- ~ 10 keV:
much longer focal lengths needed

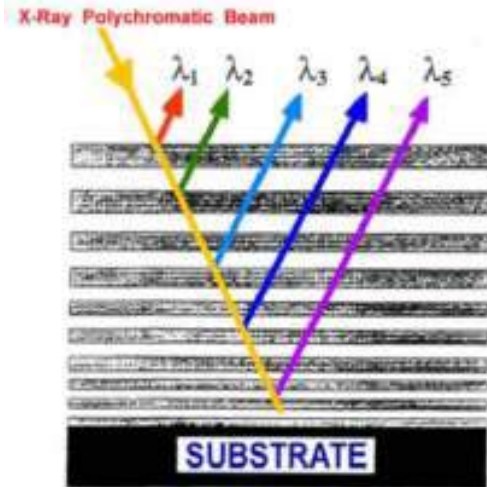
X-ray mirror performance



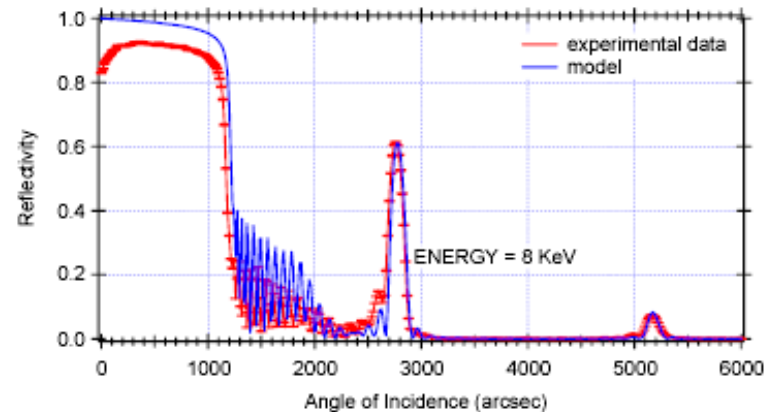
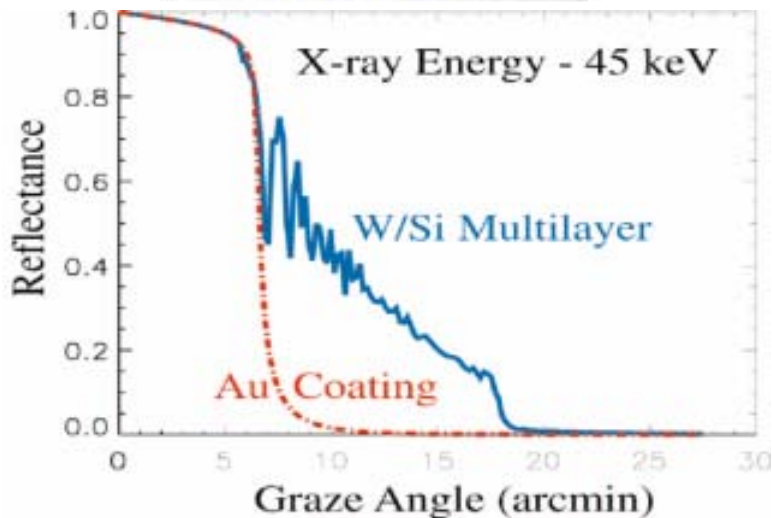
- or the difficulty to produce high-quality mirrors

- to reach higher resolutions: large increase in the Mass/Geom. Area ratio necessary

Multilayer mirrors



- Stack of alternating layers (materials of low and high Z + index of refraction)
- operating on the basis of Bragg reflection
$$n\lambda = 2d \sin \theta$$
 d = bi-layer thickness
- wide range of thickness
➔ broadband reflectance



X-ray Detectors

- Scintillation detectors
- Geiger-Müller-counter
- Proportional counters / gas detectors
- Microchannel plate detectors (MCP)
- Charge-Coupled Devices (CCD)
- Spectroscopic devices: gratings
- X-ray bolometers / calorimeters

Types of detectors/spectrometers

Detector	physical Interaction	Energy of ionization E_{ion}	$R=E/\Delta E$ @ 1 keV
Scintillator	photo-electron, inner electron	keV	-
Proportional Counter	photo-electron, noble gas	30 eV	2.5
Semiconductor Detector	Silicon, electron-hole pairs	3 eV	8
Bolometer/Calorimeter	phonons, Cooper pairs	few meV	1000
Transition Edge Sensor	heat		1000
Gratings	diffraction		> 1000

Scintillators & Photomultiplier

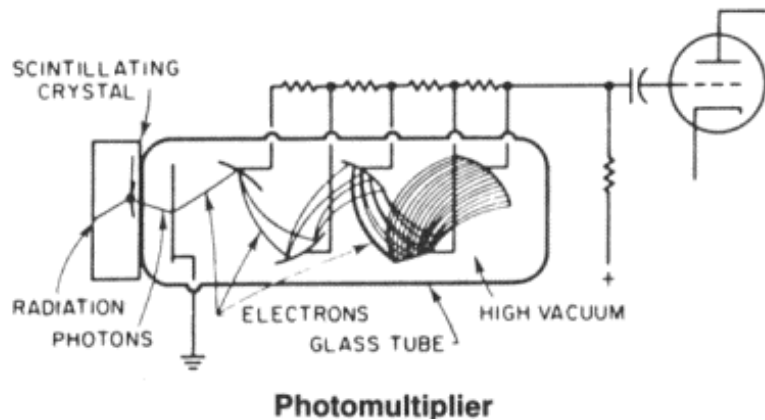


converting X-ray energy into visible light

- organic scintillators (plastics)
almost exclusively used as anti-coincidence shields
- inorganic scintillators (crystals: NaI, CsI, BGO ...)

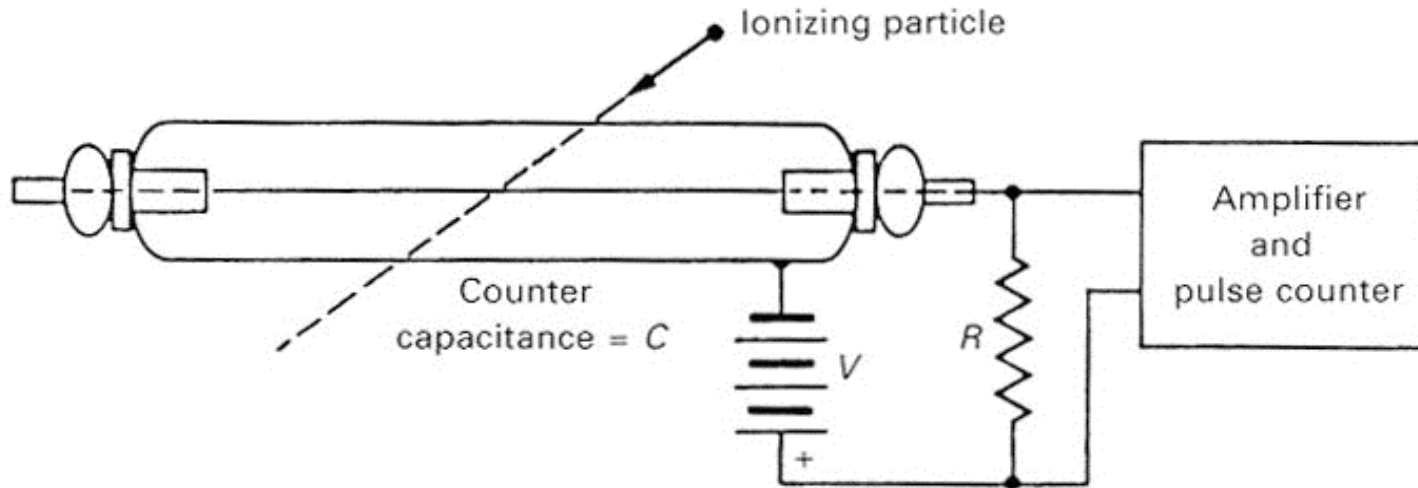
Alkali halides: NaI, CsI

- can be made into large area crystals: NaI(Tl), CsI(Na)
- good X-ray stopping power
- efficient light producers



- photo-electron creates scintillation pulse with different decay times for different materials
- total light output proportional to energy input

Geiger-Müller Counter



- windowed gas cell filled with a mixture of noble gases Ar, Xe, ... (low ionization potential)
- detection of X-rays via the photoionization of the counter gas
- ionization energy $E_{\text{ion}} \sim 30 \text{ eV}$
- photo-electrons are multiplied by high voltage acceleration
- events are counted by electric charge pulses at the output amplifier containing information on:
 - the energies
 - arrival times
 - interaction positions of the X-ray photons

Typical Proportional Counters

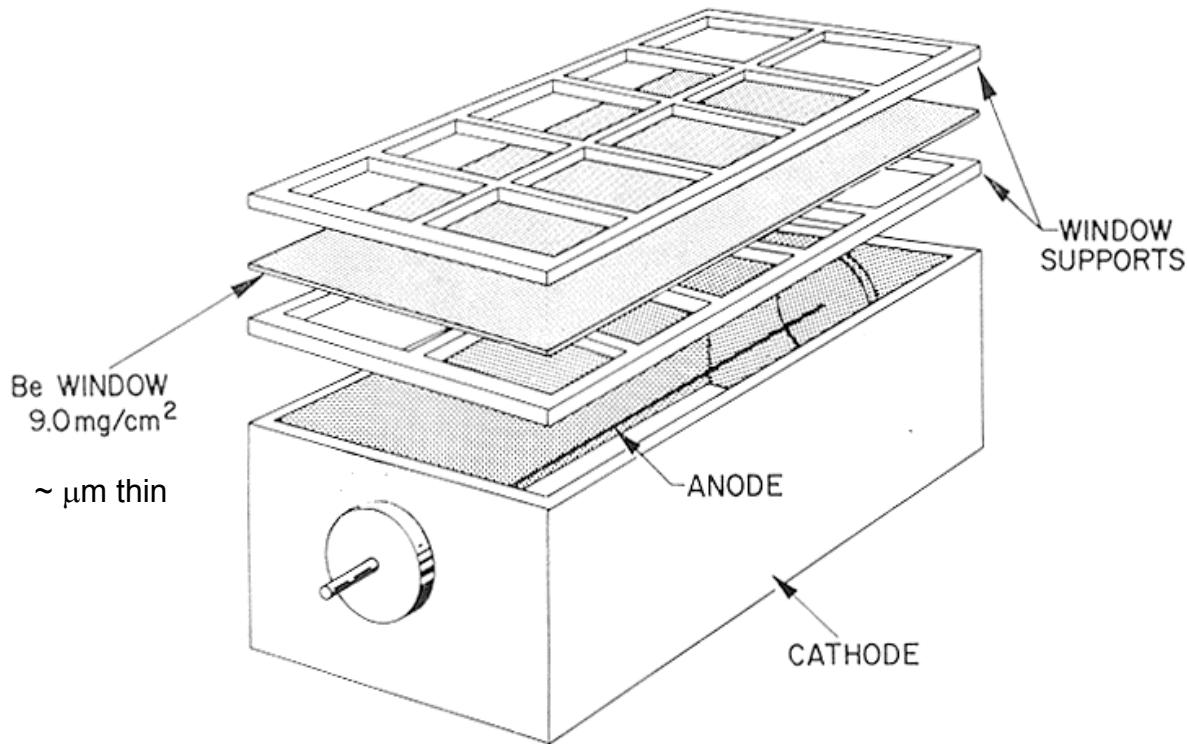


Fig. 2.10. Schematic layout of a thin window gas proportional counter. The Be window is cemented between a supporting 'sandwich' which in turn is hermetically sealed to the cathode to preserve the gas integrity. The anode is usually kept under tension by a spring. The charge sensitive preamp and high voltage power supply are ideally mounted as close as possible to the anode feed-through.

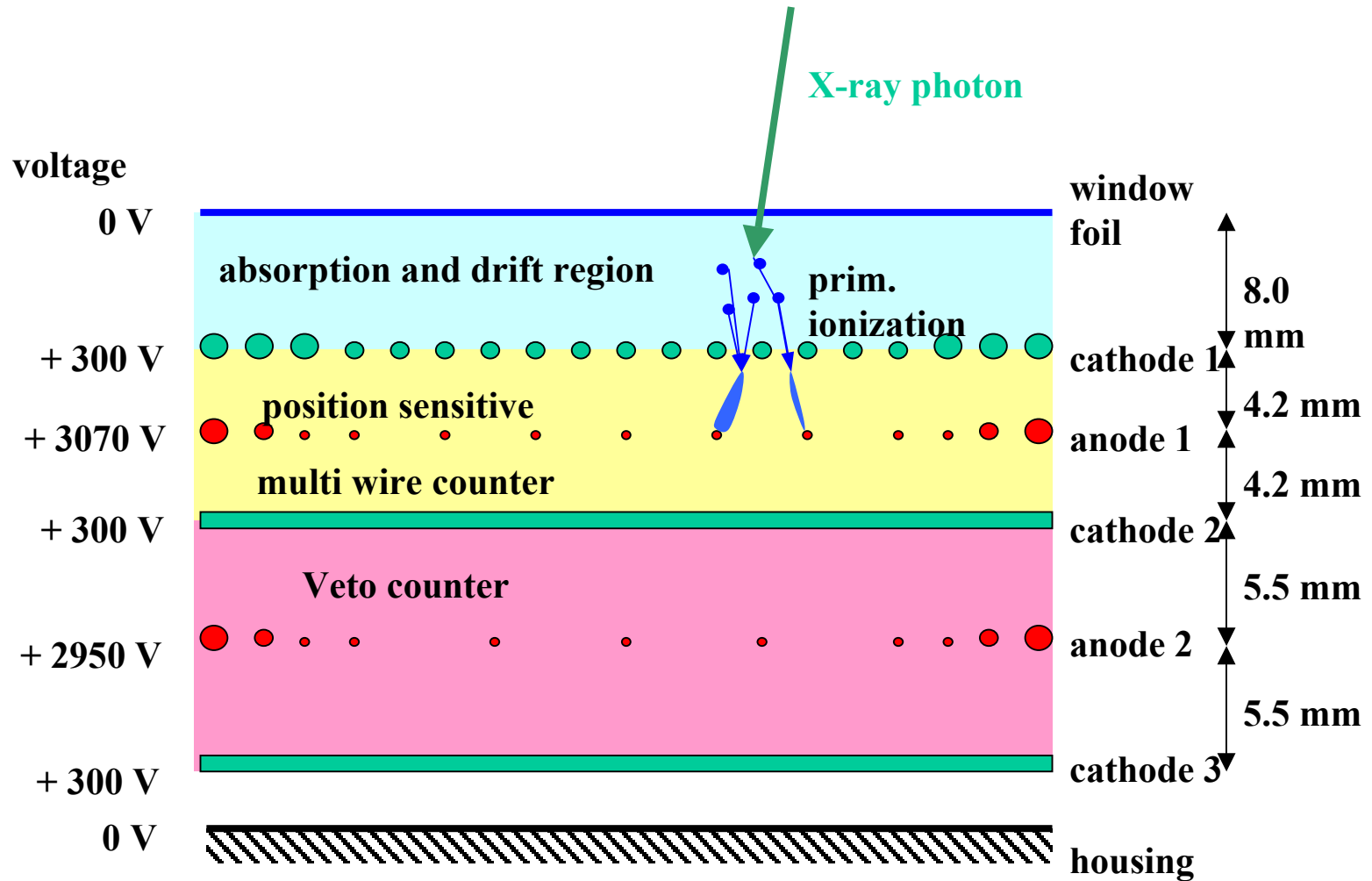
Background rejection methods

- Energy selection
reducing the raw background rates by a factor 100
- Rise-time discrimination
less effective as the X-ray energy increases (@ 6 keV: factor 30)
- Anti-coincidence with a sub-divided gas cell
reducing the raw background rates by a factor 100

Intrinsic timing resolution limited by

- anode-cathode spacing
 - positive ion mobility
- ➔ microsecond level

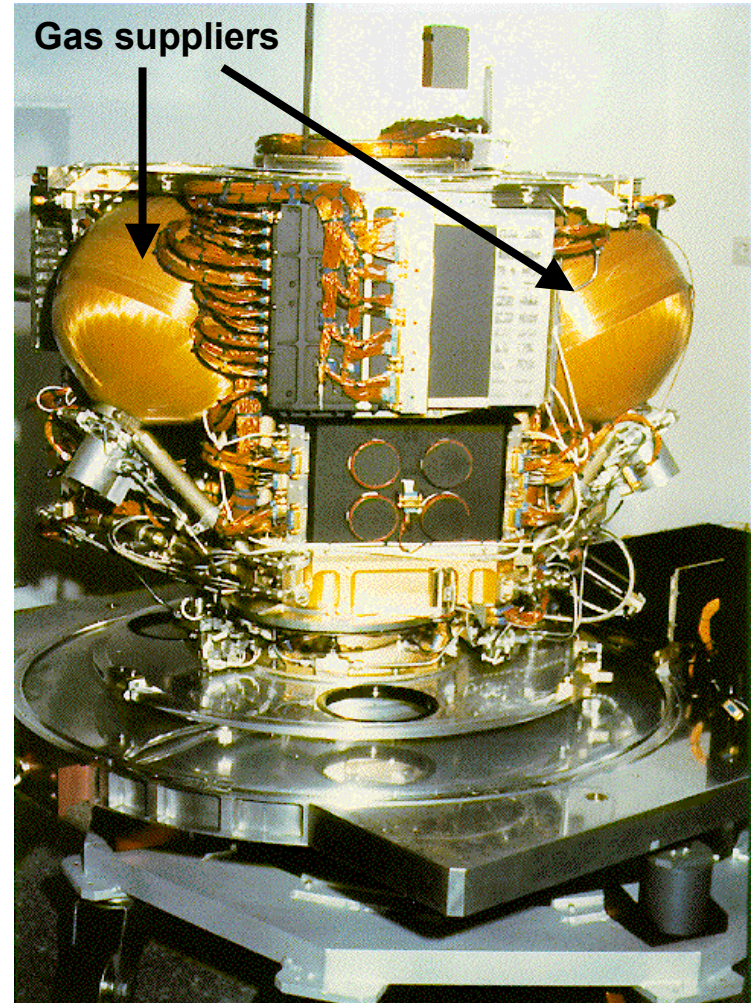
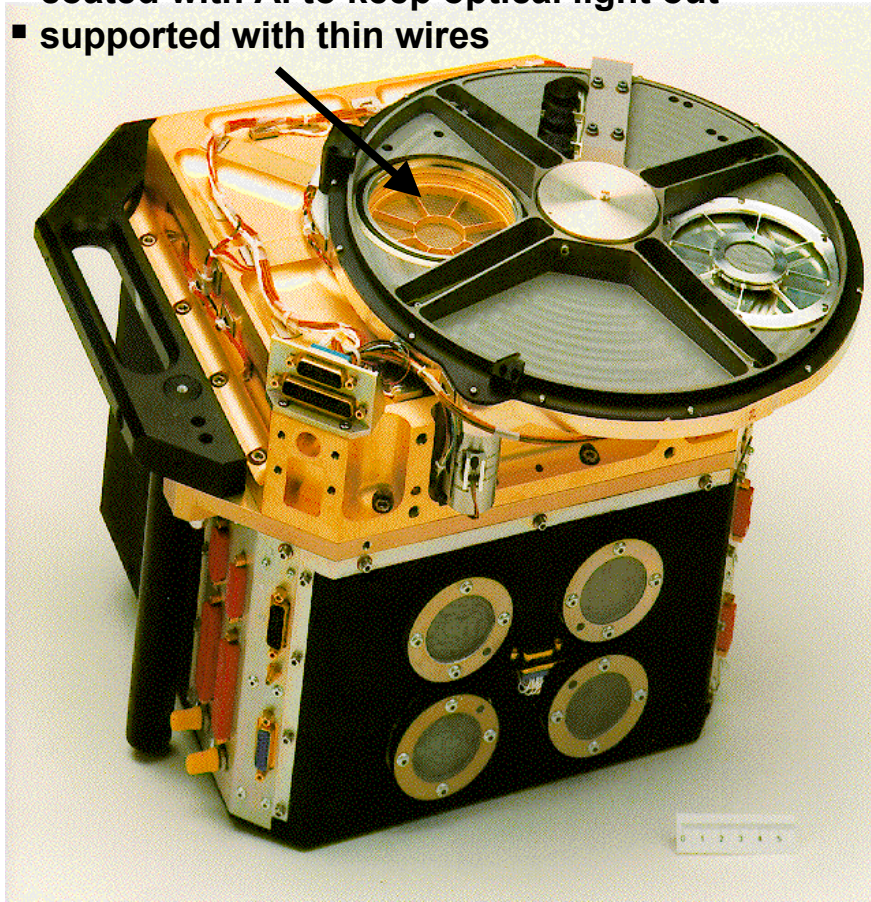
MULTIWIRE DETECTORS



The ROSAT PSPC

~ μm thin plastic entrance window

- coated with Al to keep optical light out
- supported with thin wires



Microchannel plate detectors

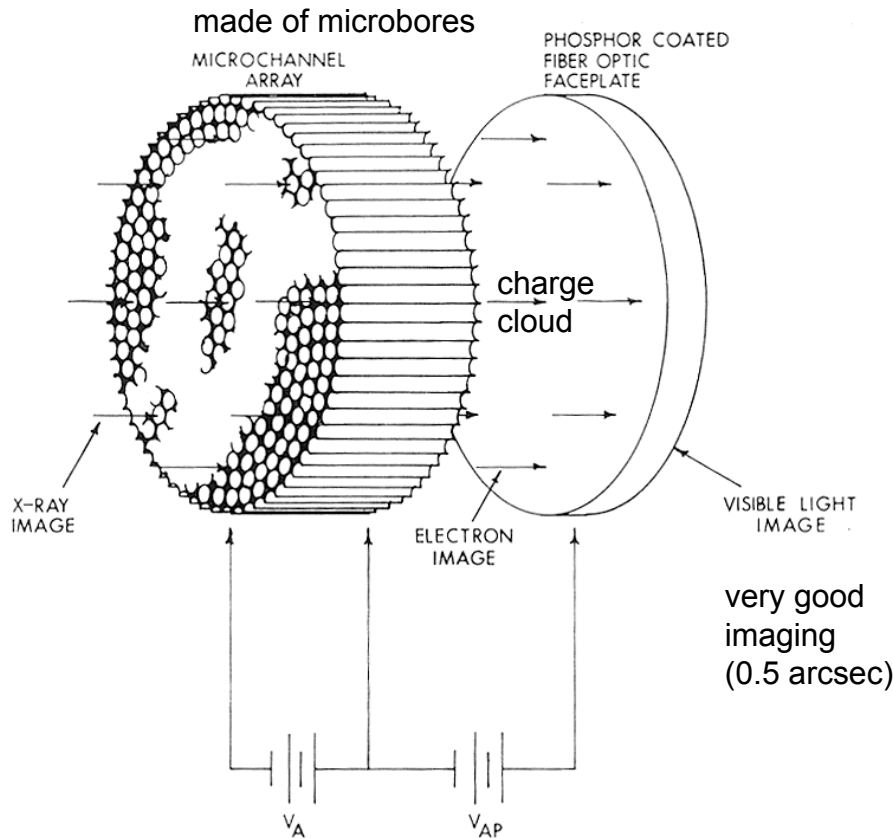


Fig. 2.15. Two dimensional channel multiplier array, used as an X-ray image intensifier. The X-ray image is converted to an electron image inside the entrance walls of the microchannel array. The bias V_A along the array multiplies these electrons, while the channel structure preserves the image. The resulting electron image is accelerated by V_{AP} to produce a visible image on a phosphor screen.

- compact electron multipliers of high gain
- consists typically of $\sim 10^7$ closed packed channels of common diameter ($\sim 10 \mu\text{m}$)
- each channel acts as an independent, continuous dynode photomultiplier
- usage: distortionless imaging with very high spatial resolution

Physical principle

- X-rays are being converted into photoelectrons
- acceleration and multiplication through a voltage gradient in the channel
- electron cloud hits a phosphor plate, inducing emission of visible photons
- position-measure of the incident photon
- energy resolution = 0 ($\Delta E/E = 1 @ 1 \text{ keV}$)
- present on Einstein(HRI), ROSAT(HRI) and Chandra

The Chandra HRCs

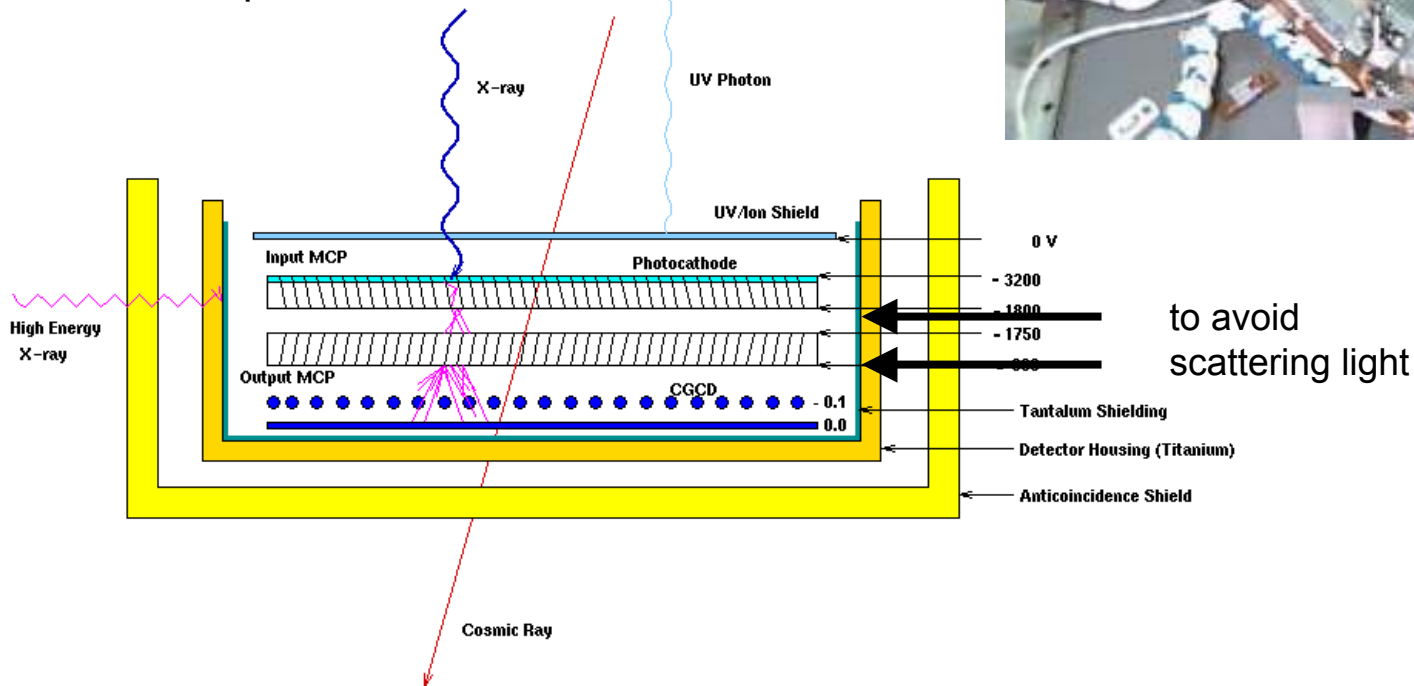
2 microchannelplate detectors (0.1 – 10.0 keV)

■ HRC-I

- one 90 mm square detector
- effective area: 225 cm² @ 1 keV
- ~ 0.5 arcsec spatial resolution

■ HRC-S

- one 20x300 mm rectangular detector
- optimized for use with the LETG



Semiconductor detectors - Charge-Coupled Devices (pn-CCDs)

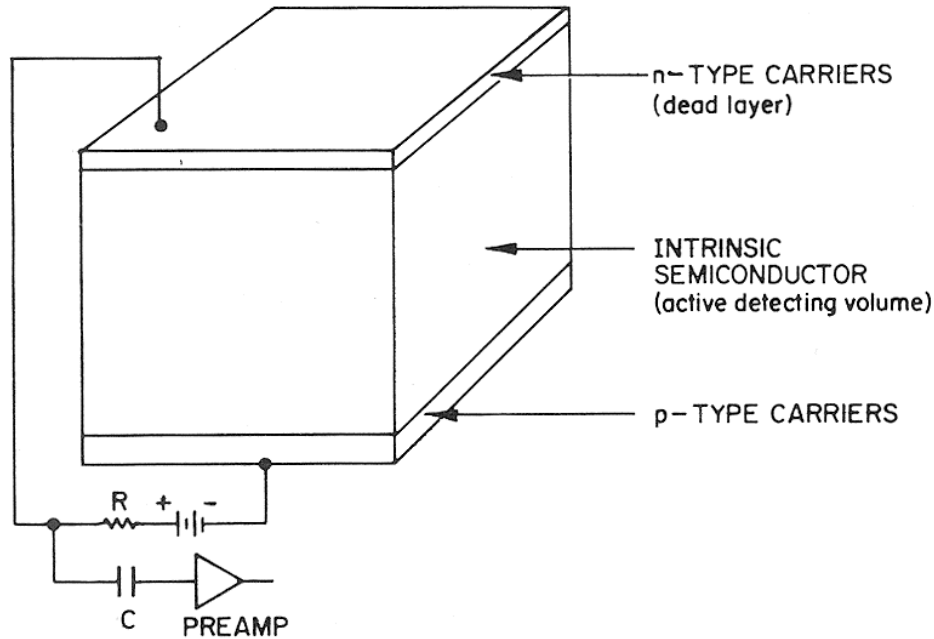


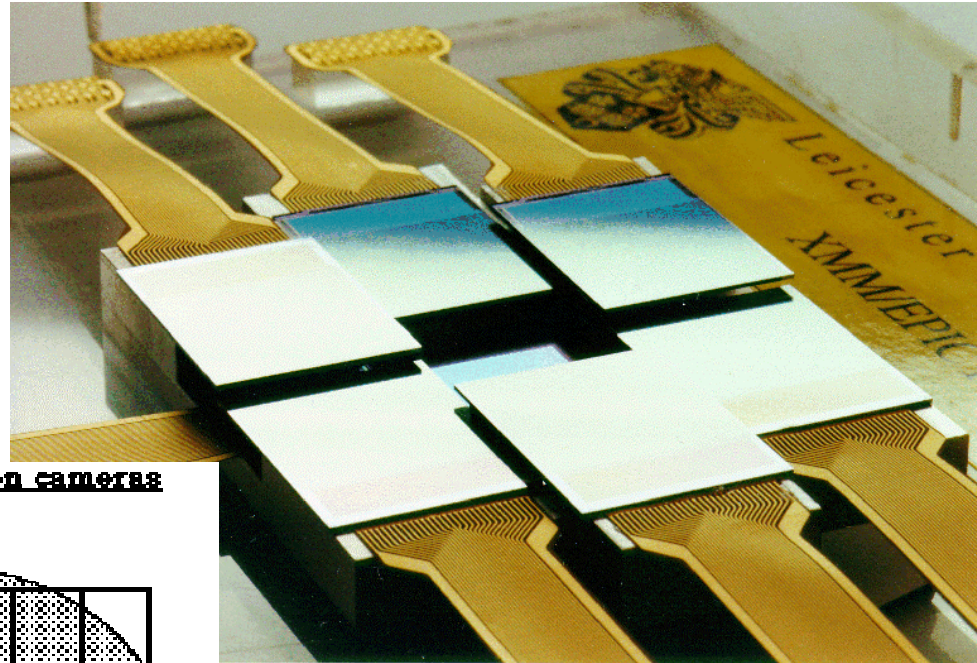
Fig. 2.14. Functional diagram of a semiconductor detector. A semiconductor crystal such as Ge or Si is doped to control the charge carrier densities. A thin layer of electron (*n*-type) carriers and a layer of 'hole' (*p*-type) carriers serve as the bias contacts. The intrinsic region has equal negative and positive carrier densities and hence can sustain the electric field across its depth. Interactions in the intrinsic layer produce electrons which can be collected in this field, exactly analogous to ionization chamber operation.

Si energy band gap = 1.1 eV
 average efficiency => 3.5 eV/reaction

- solid-state imager
- higher quantum efficiency than counters, but more noisy (cooling)
- high purity Si doped on both sides with *n*-carriers and *p*-carriers
- incoming photon excites electrons into the conduction band
- number of sensitive material strips corresponding to number of read-out electrodes („pixel“)
- accumulation of charge in the pixels
- transfer to successive electrodes and read-out by separate row amplifiers

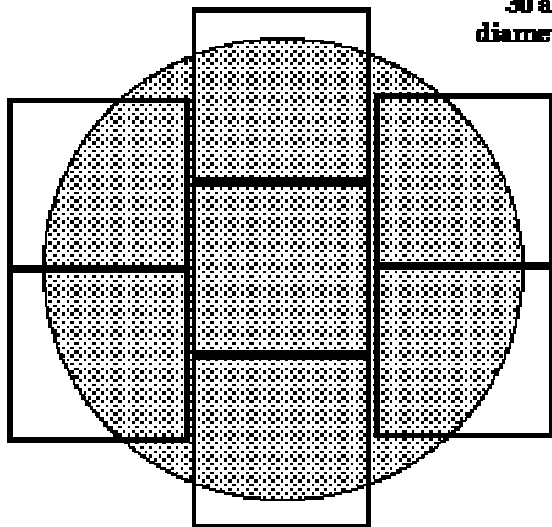
XMM-Newton EPIC MOS-CCD

- European Photon Imaging Camera (EPIC), made of Metal-Oxide-Silicon
- 2 x Arrays of 7 CCDs each (0.1 – 10.0 keV)
- each CCD consists of 600 x 600 pixels
- $E/\Delta E = 20 - 50$
- pixel size: $40 \times 40 \mu\text{m}^2$ (1.1 arcsec)²
- field of view: 30 arcmin diameter



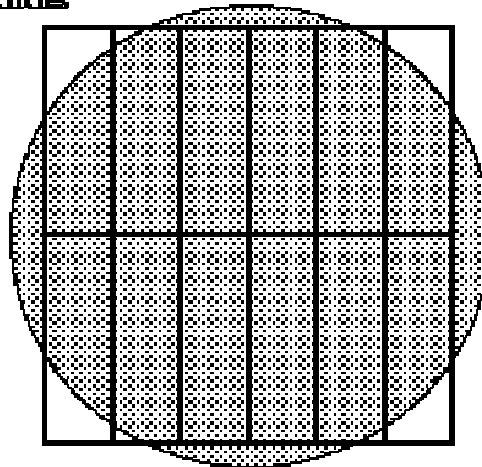
Comparison of focal plane organisation of EPIC MOS and pn cameras

30 arc min
diameter circles



EPIC MOS

7 CCDs each 10.9×10.9 arcminutes

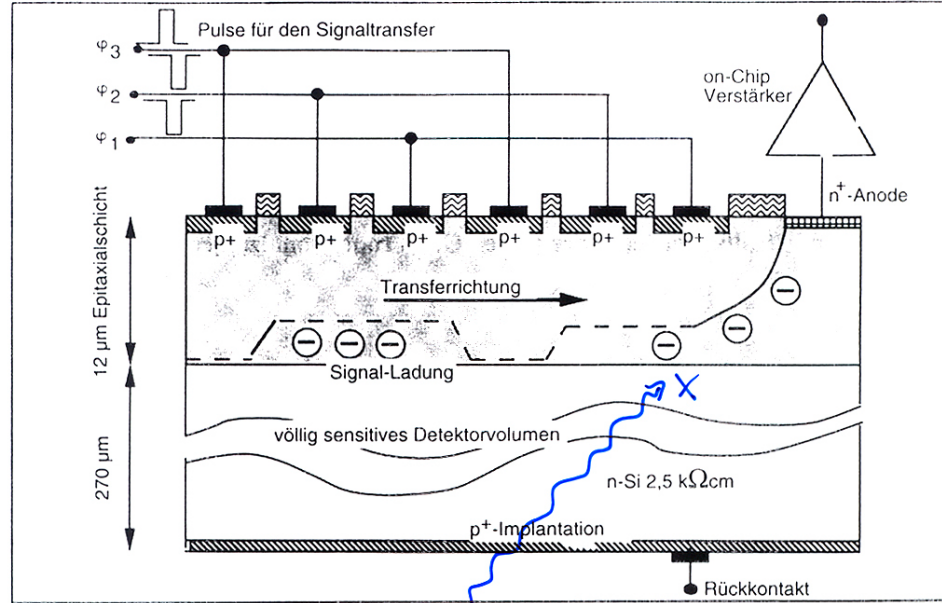
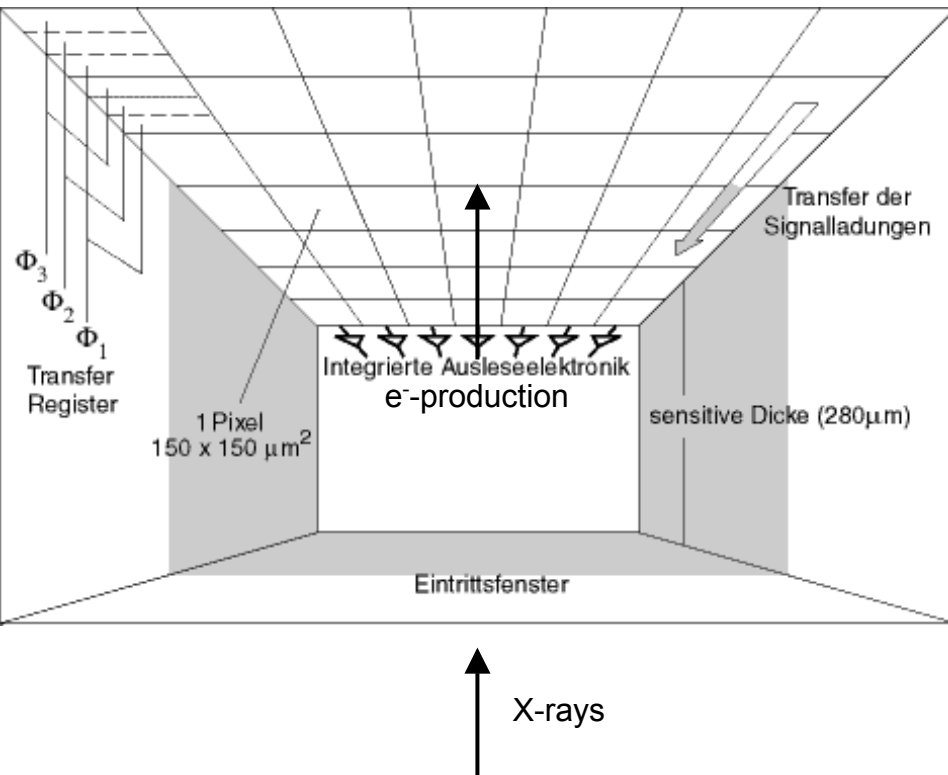


EPIC pn

12 CCDs each 13.6×4.4 arcmin

pn-CCD Operating Principle

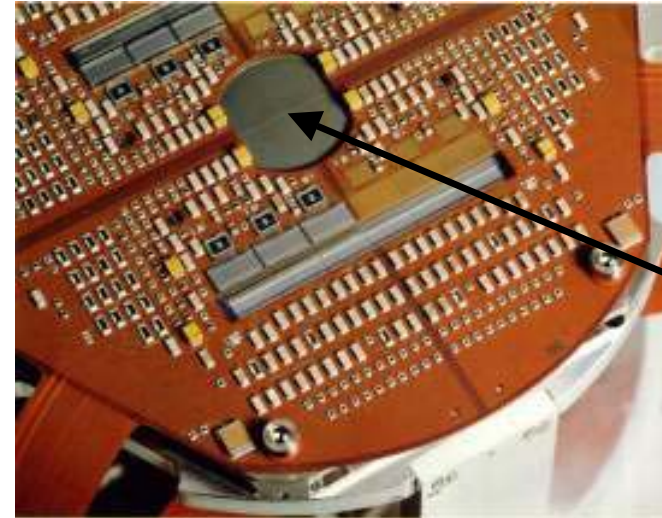
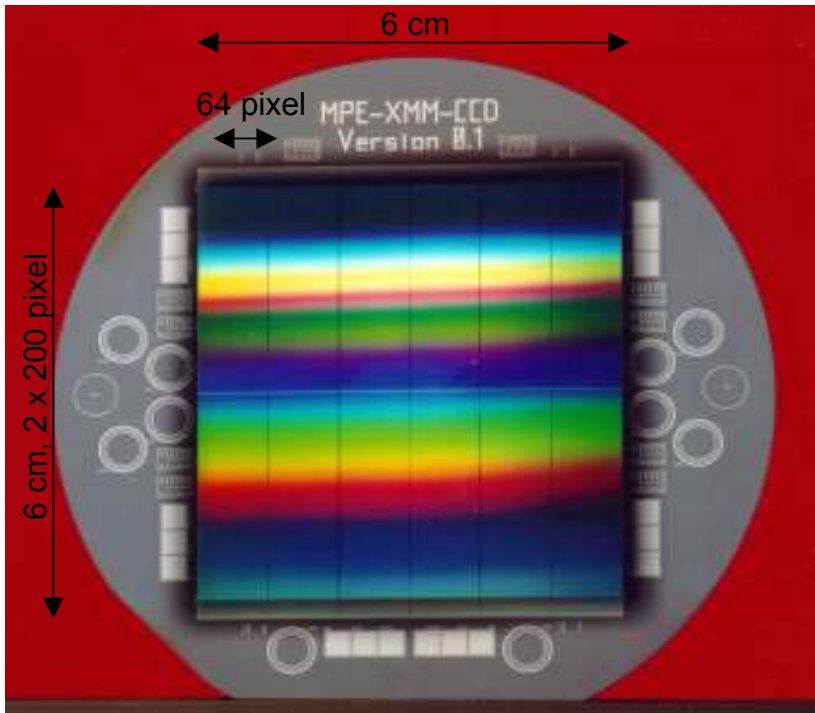
view from inside the CCD, from the n-side



- applying an electric field in the Si sensitive region
- transfer of the created charges to the gate
- cycling the voltages of the electrodes
 - ➡ move of the charges to the read-out

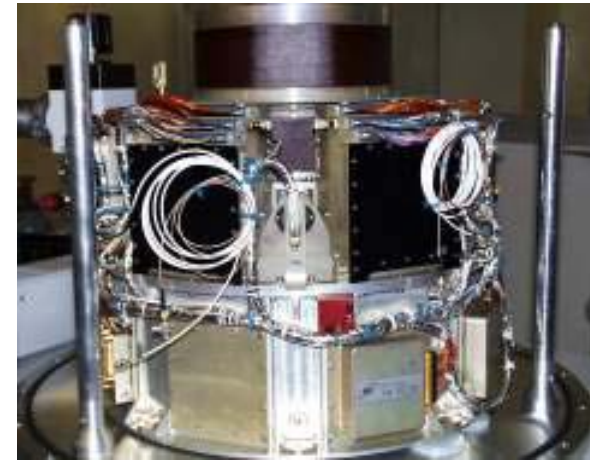
XMM-Newton EPIC pn-CCD

- European Photon Imaging Camera (EPIC)
- array of 12 back-illum. CCDs (0.1 – 15.0 keV)
- $E/\Delta E = 20 - 50$
- field of view: 27.5 arcmin diameter
- pixel size: $150 \times 150 \mu\text{m}^2$ (4 arcsec)²



Electronic board with 64 amplifiers

Front side



Cooling device
($T \sim -80$ to -90 K)

Bragg Crystal Spectrometer

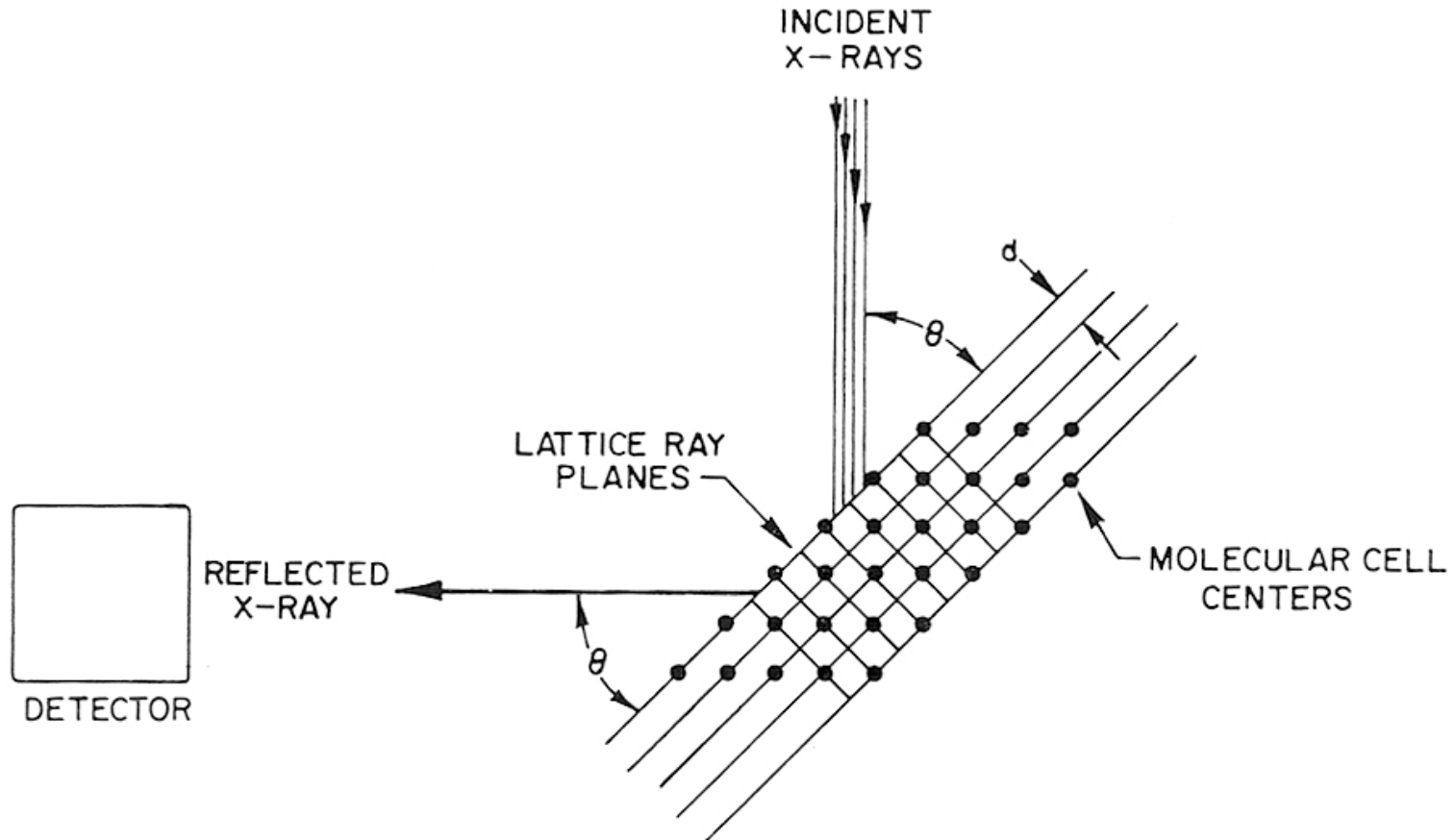


Fig. 2.25. Any set of lattice planes with spacing d will Bragg scatter radiation incident at a direction θ from those planes within a narrow range of wavelengths satisfying $n\lambda = 2d \sin \theta$. The total counting rate of the detector as the angle θ is varied gives the relative spectrum as a function of λ .

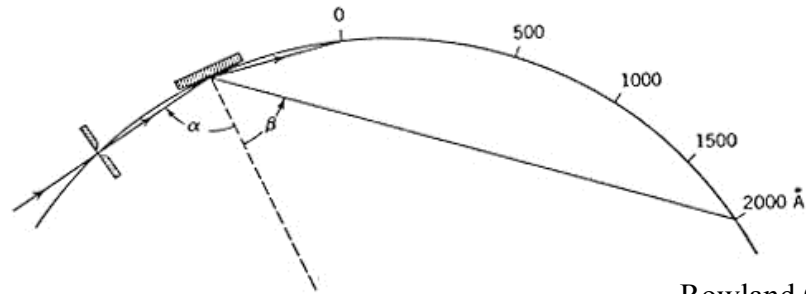
Why High Dispersion Spectroscopy?

High dispersion spectroscopy can resolve emission lines that may be used to study:

- the physical conditions (T,N) by comparing lines from the same ion
- the ionization balance (lines from different ions of the same element)
- the chemical abundances (lines from different elements)
- the radial velocity and red-shift

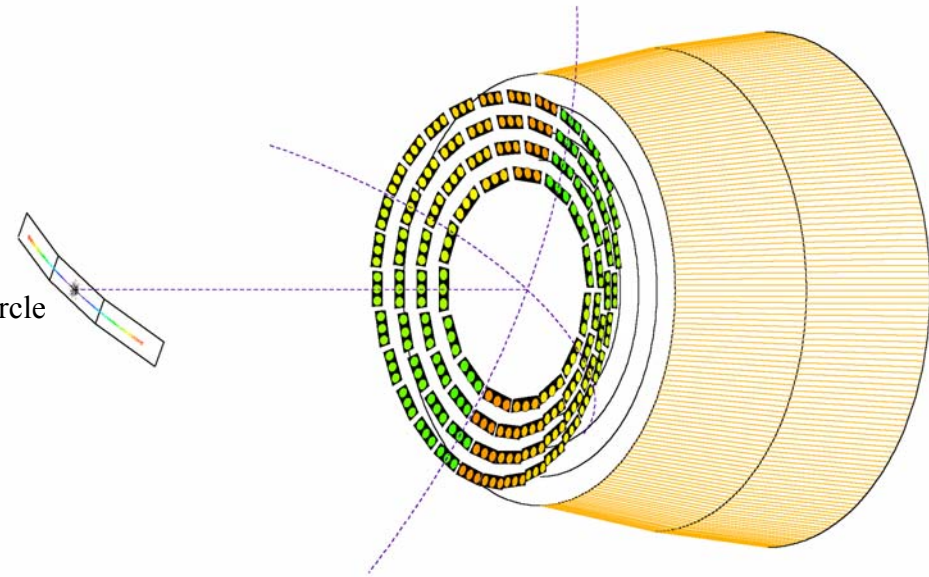
Each diagnostic requires a characteristic resolving power, $R = E/\Delta E = \lambda/\Delta\lambda$

Grating Spectroscopy



Grazing incidence spectrograph.

Rowland Circle



Reflection grating

Transmission grating

Reflection at grazing incidence angles
by a grating

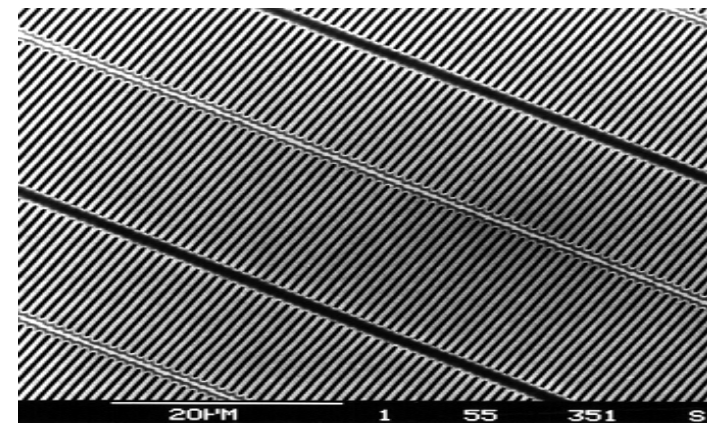
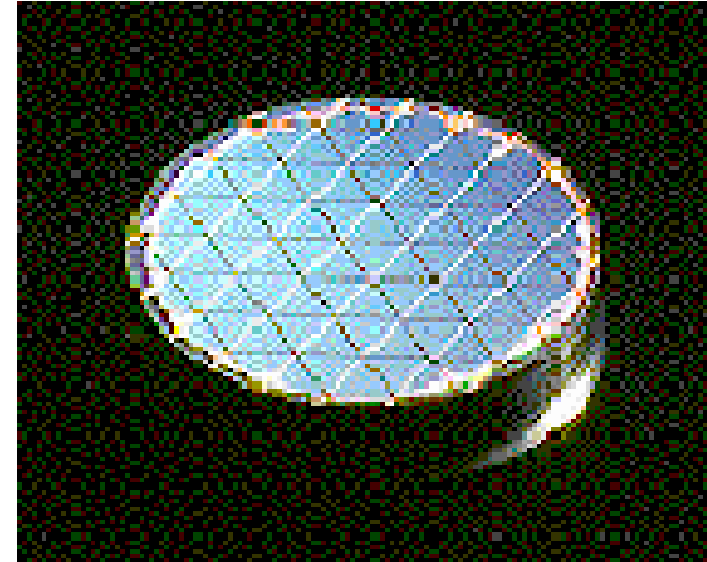
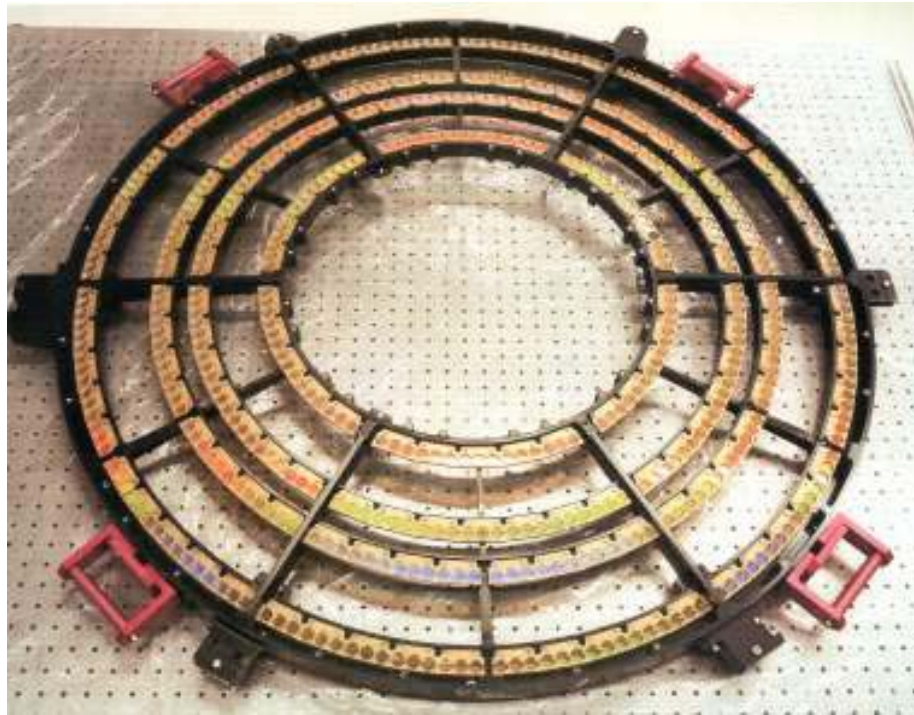
Transmission spectrometers

- = circles, each with a little transmission grating
- mounted on a Wolter telescope

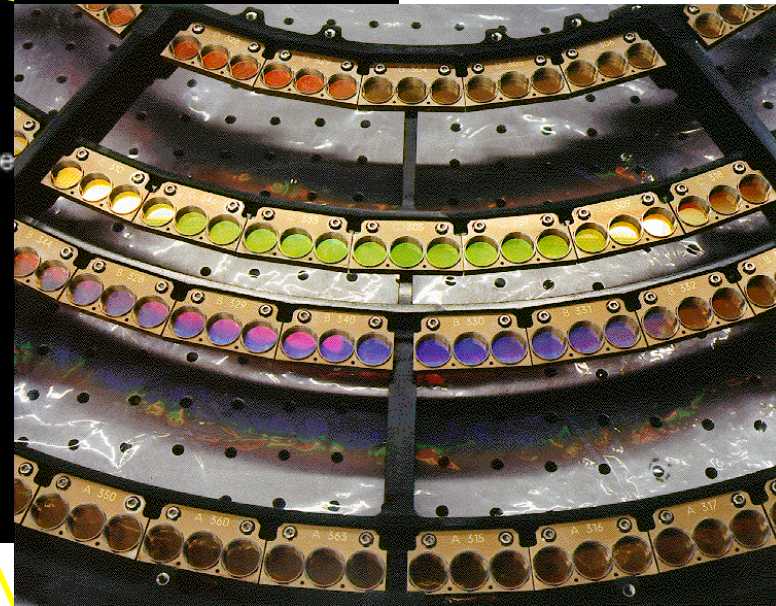
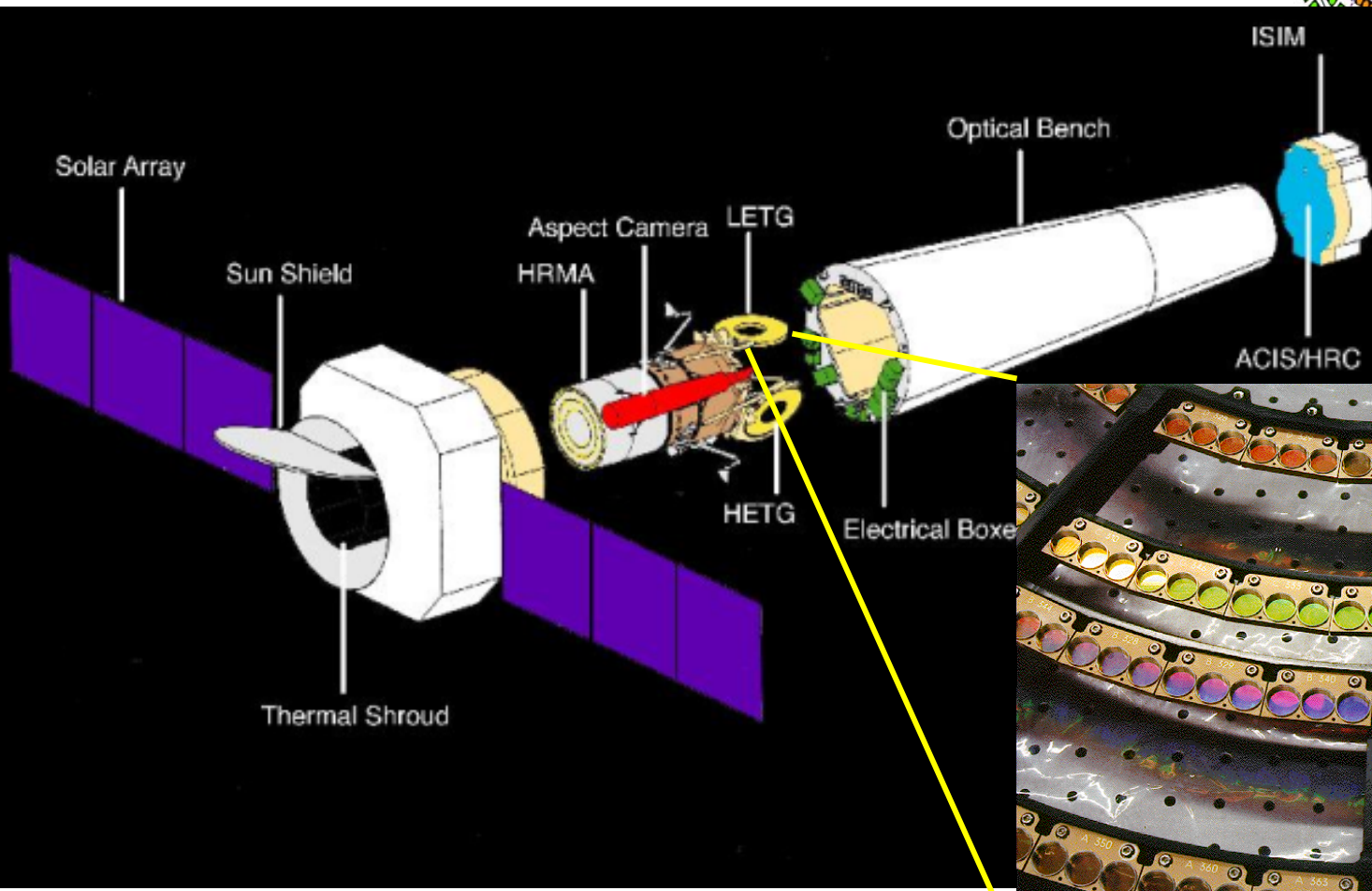
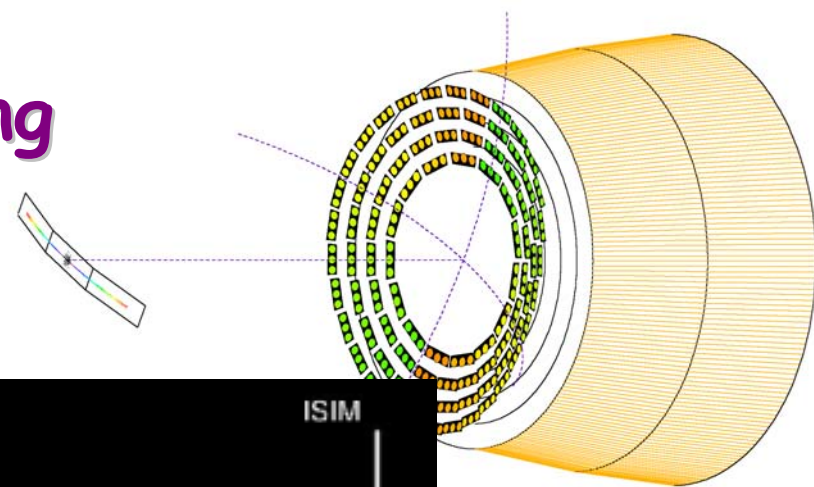
⁺ (Adapted from Samson, J., "Techniques of Vacuum Ultraviolet Spectroscopy", John Wiley & Sons, 1967)

Chandra Transmission Grating LETG

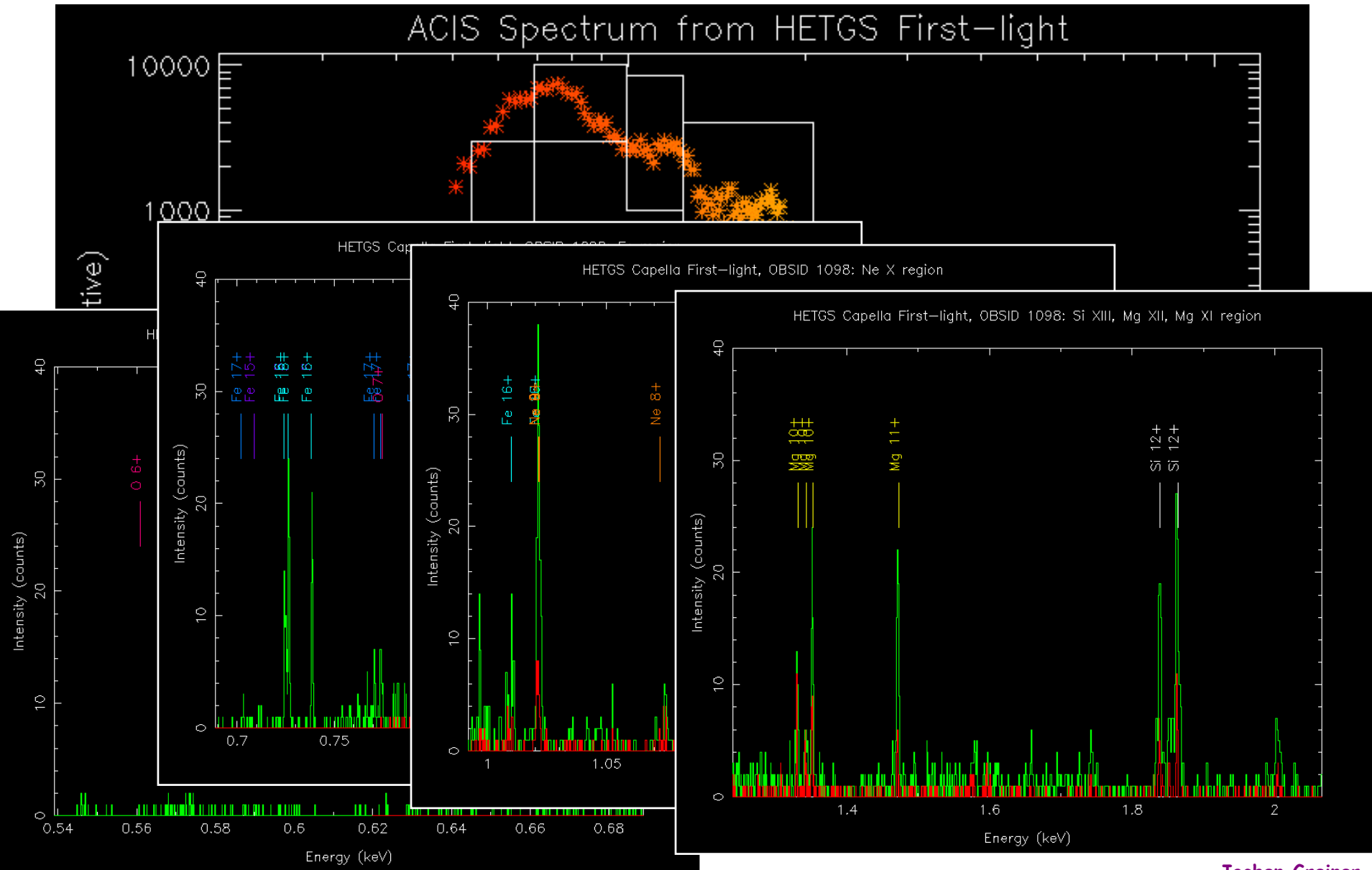
- grating material: free standing gold wires ($0.5 \times 0.5 \mu\text{m}^2$) on a supporting mesh
- diameter of each grating facet: 1.6 cm
- facet frame material: stainless steel
- 540 single grating facets mounted on a ring shape frame



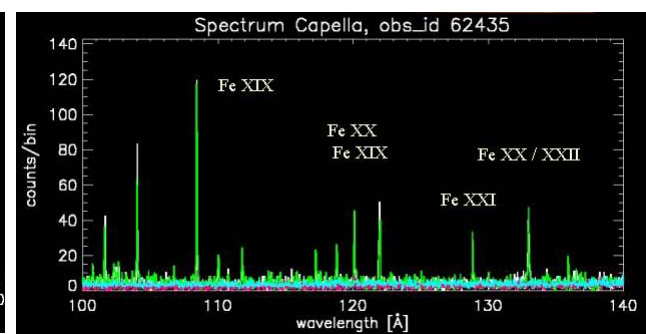
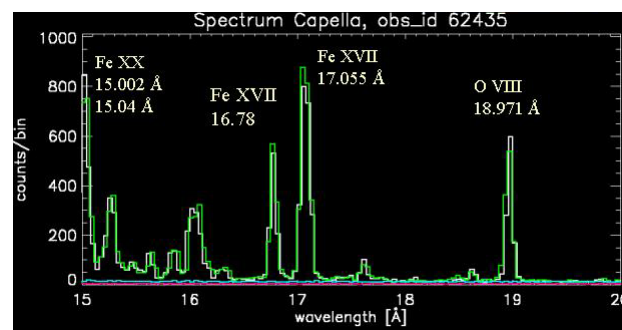
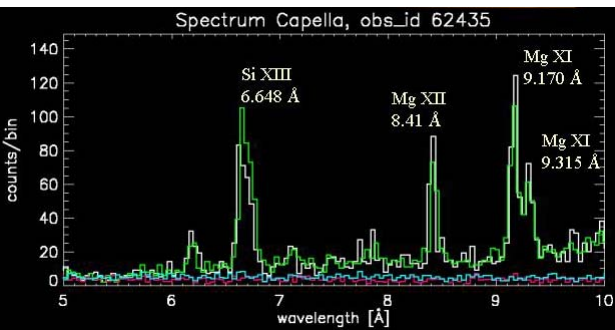
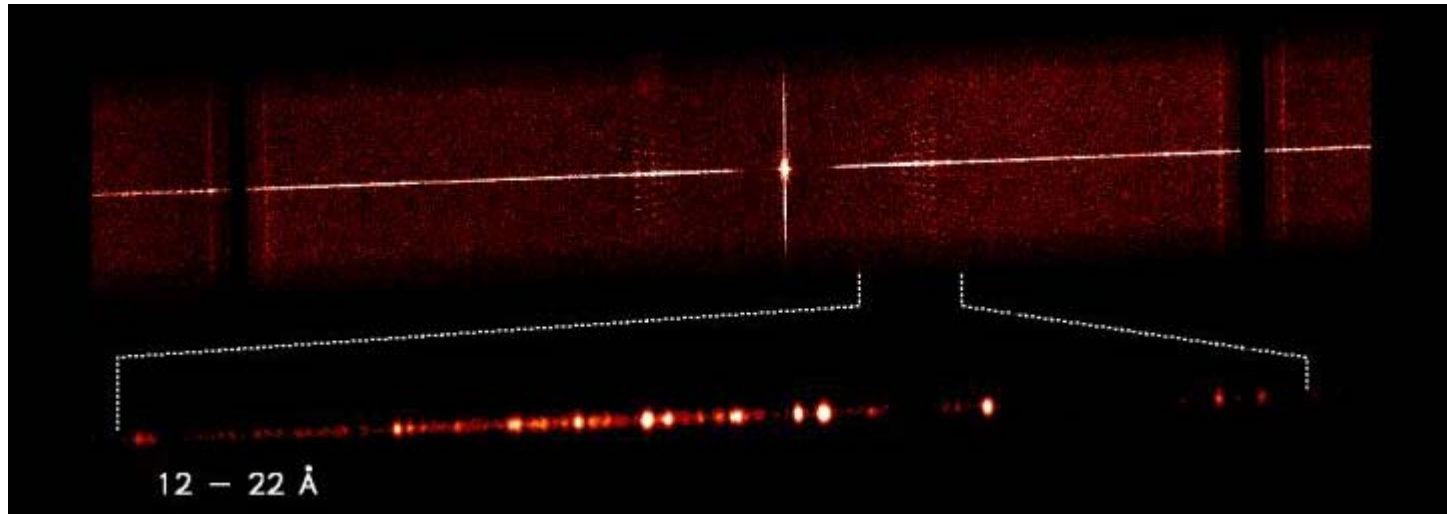
Chandra Transmission Grating



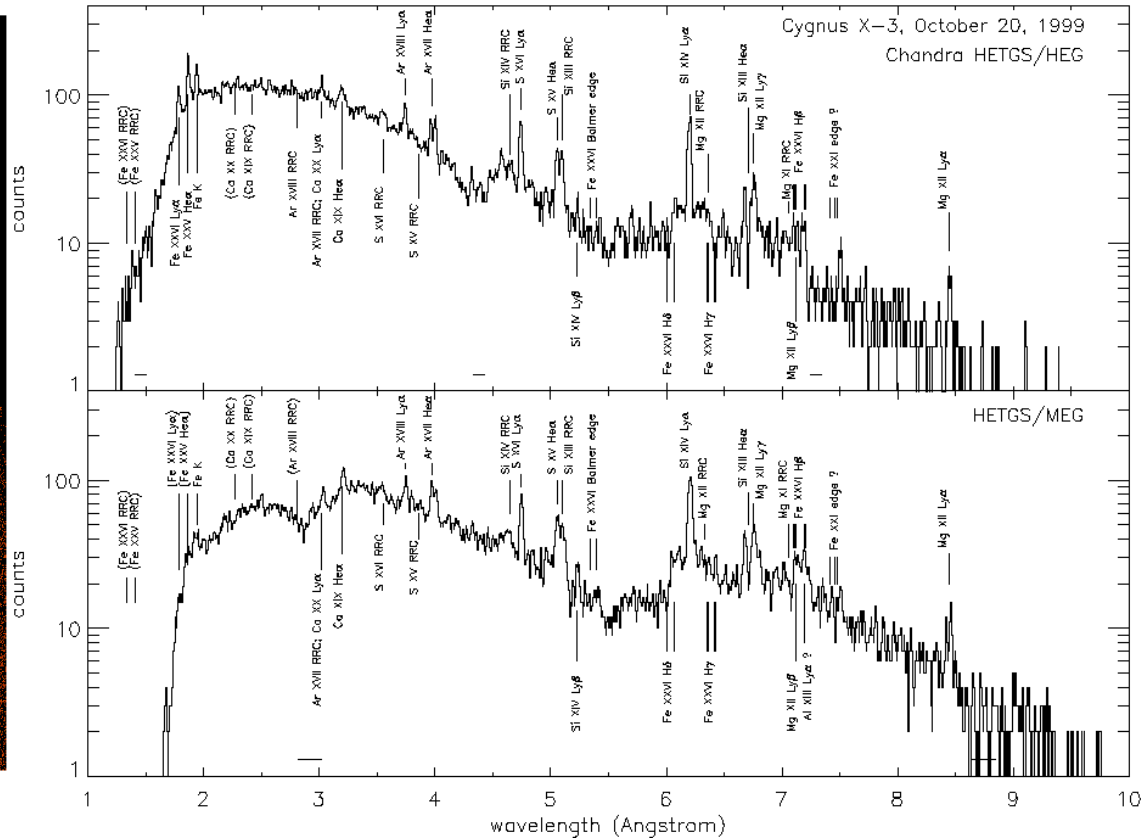
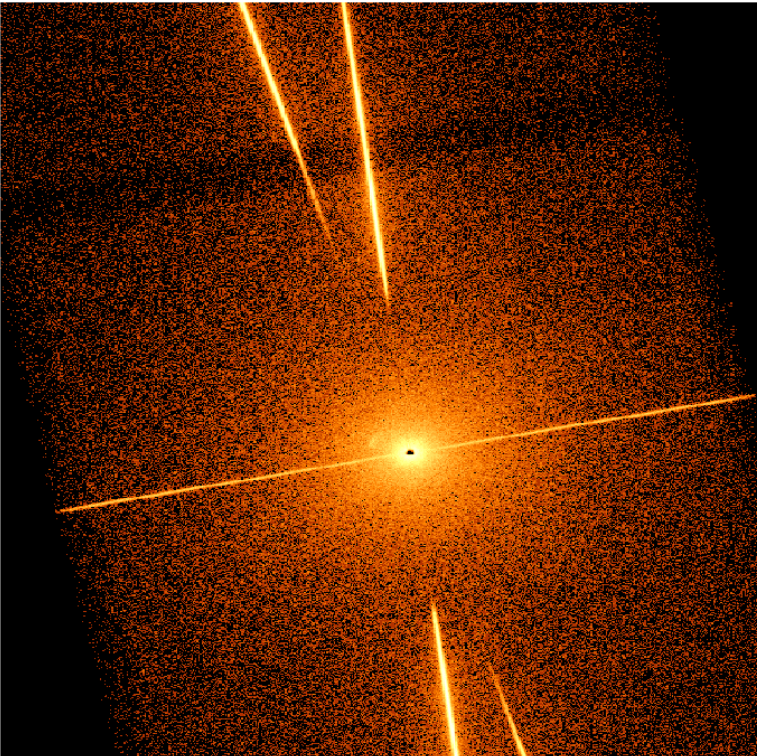
Non-Diffractive vs Diffractive X-ray Spectroscopy



LETG Capella

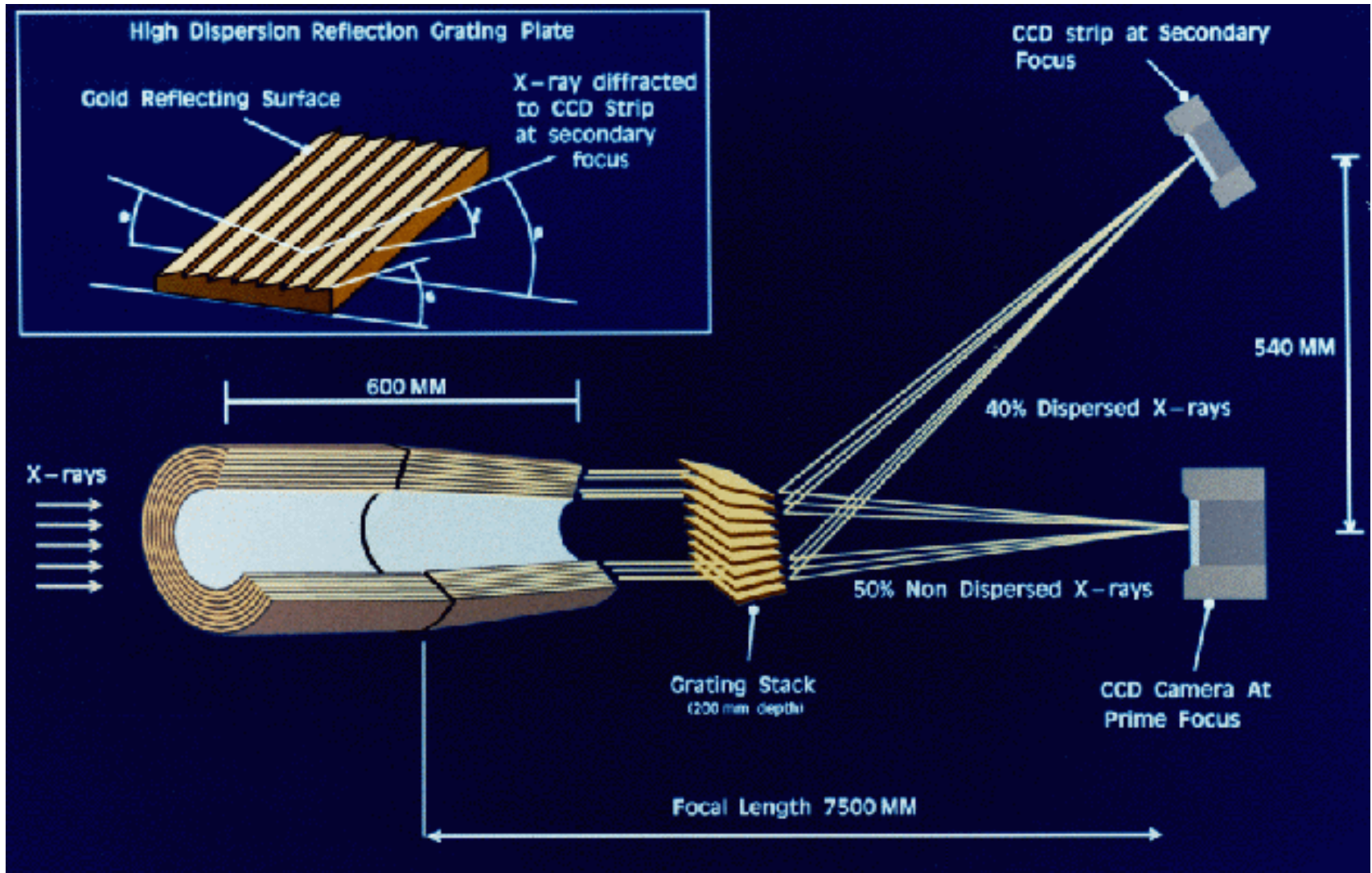


Chandra Grating Spectroscopy of Cyg X-3

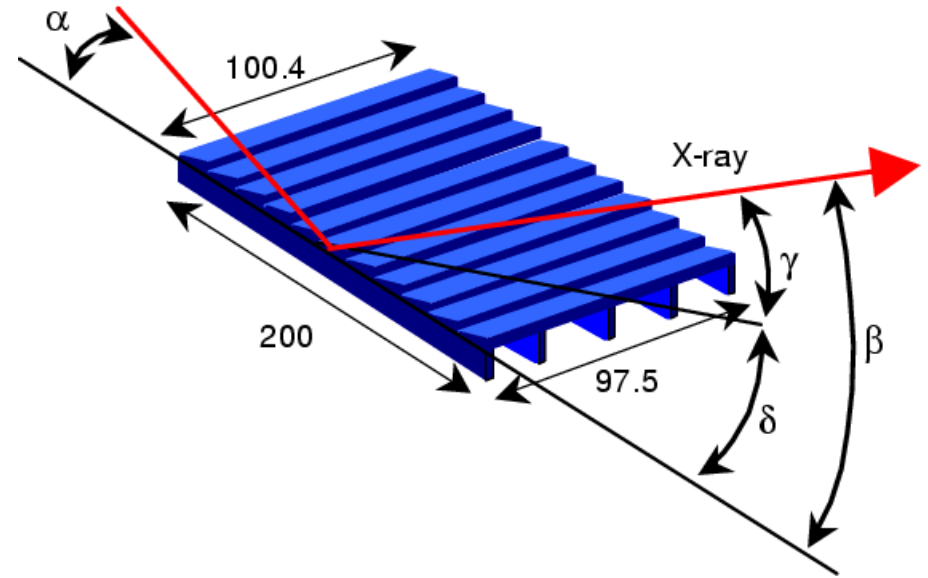
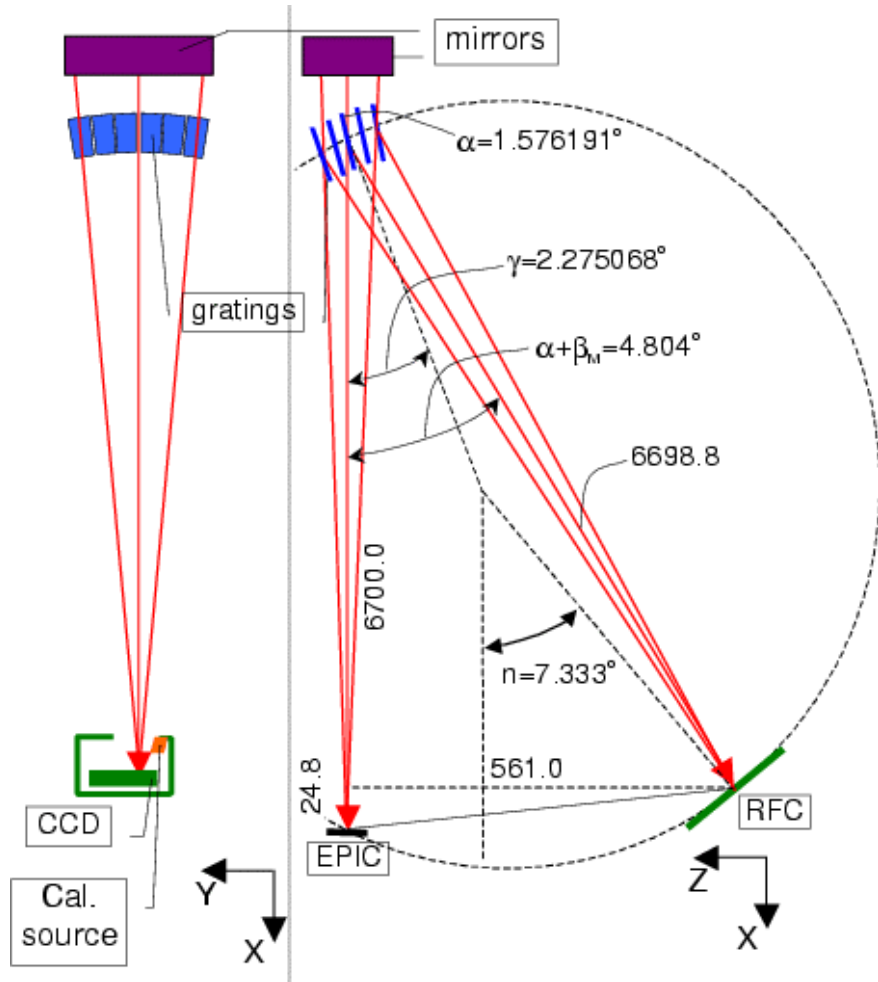


A revolution in X-ray astronomy !

XMM-Newton reflection grating



XMM Reflection Gratings



$$\sin \beta = \kappa / D$$

$$\Delta \kappa \nleftrightarrow \Delta \beta = \text{const.}$$

Looking ahead: Future developments

- Bolometer/calorimeter
thermal X-ray detectors
- Transition Edge Sensors (TES)
- The DEPFET principle

Bolometers/Calorimeters

thermal X-ray detectors

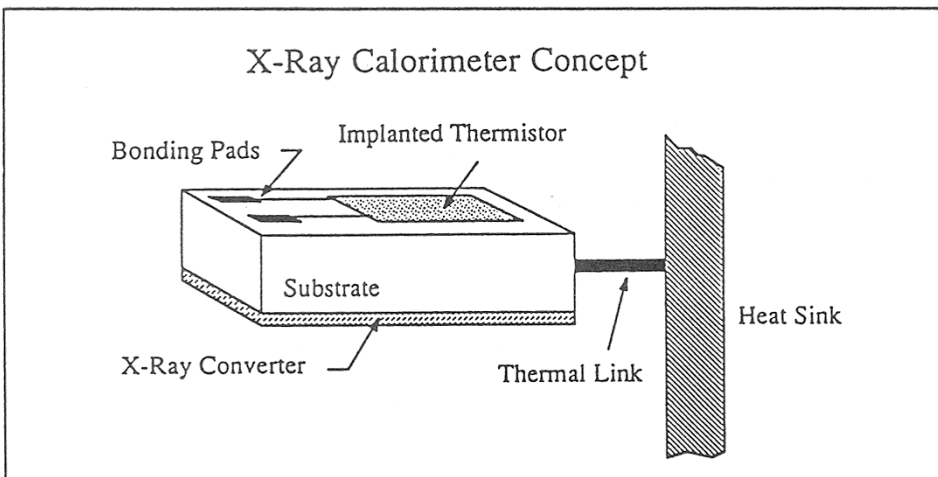
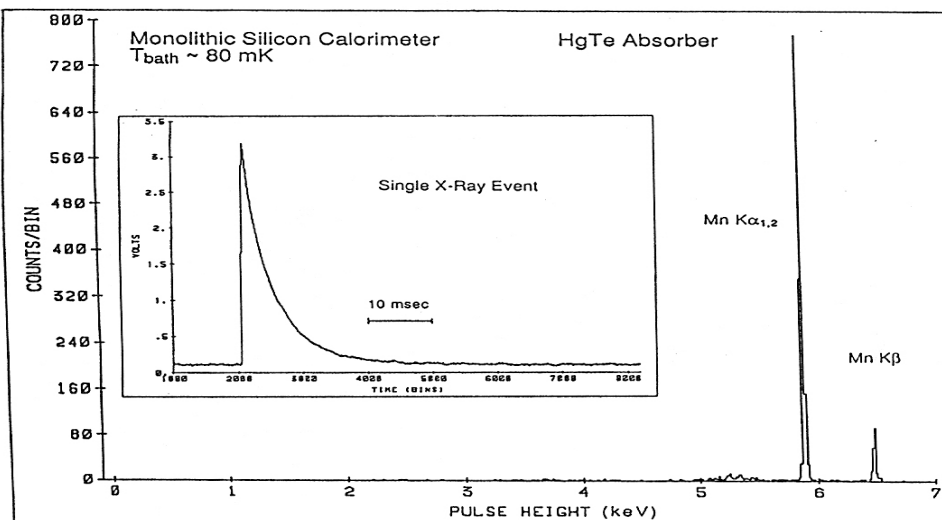
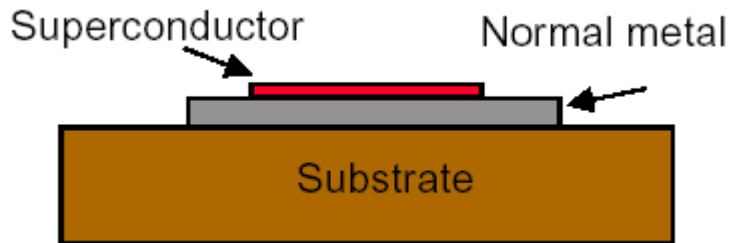


Figure 1: Schematic of the X-ray calorimeter concept.

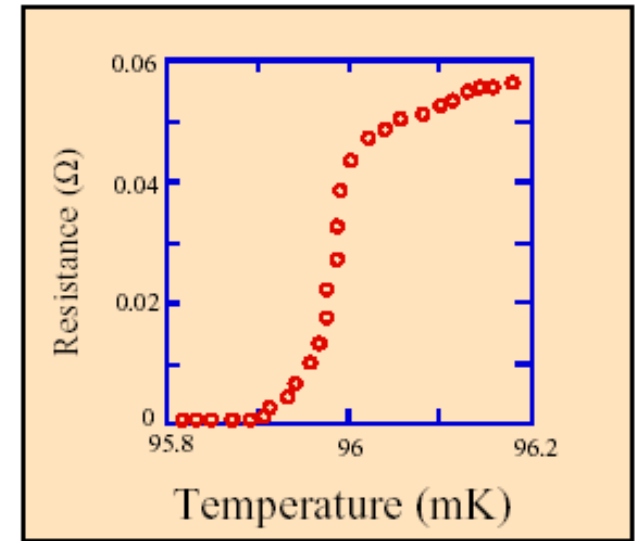


- energy of an incoming photon directly converted into thermal agitation of a crystal lattice or of an electron gas
- amplitude of the thermal impulse proportional to its energy
- ➔ **measure the temperature variation**
- for arrival times of photons larger than the characteristic time constant of the bolometer
- ➔ **discrimination of individual events**
- system must be cooled to very low temperatures ($\sim 1 \text{ mK}$., mech. refrigerator)

Transition-Edge Sensors (TES)

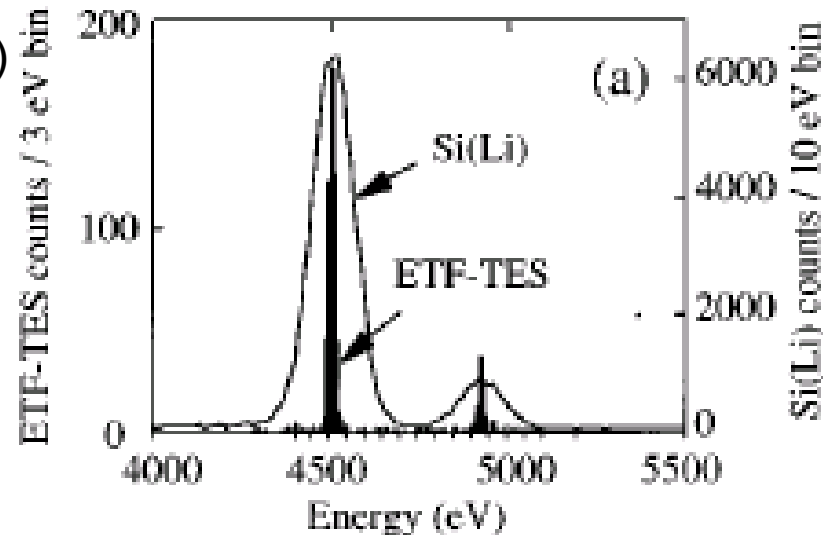


- bolometer = absorber of radiation + thermometer (with a cooling device)
- one type of thermometer: TES
- TES = strips of superconducting material
- ~ 96 mK: strong increase in resistivity
 - ▶ decrease in current (for a given voltage)



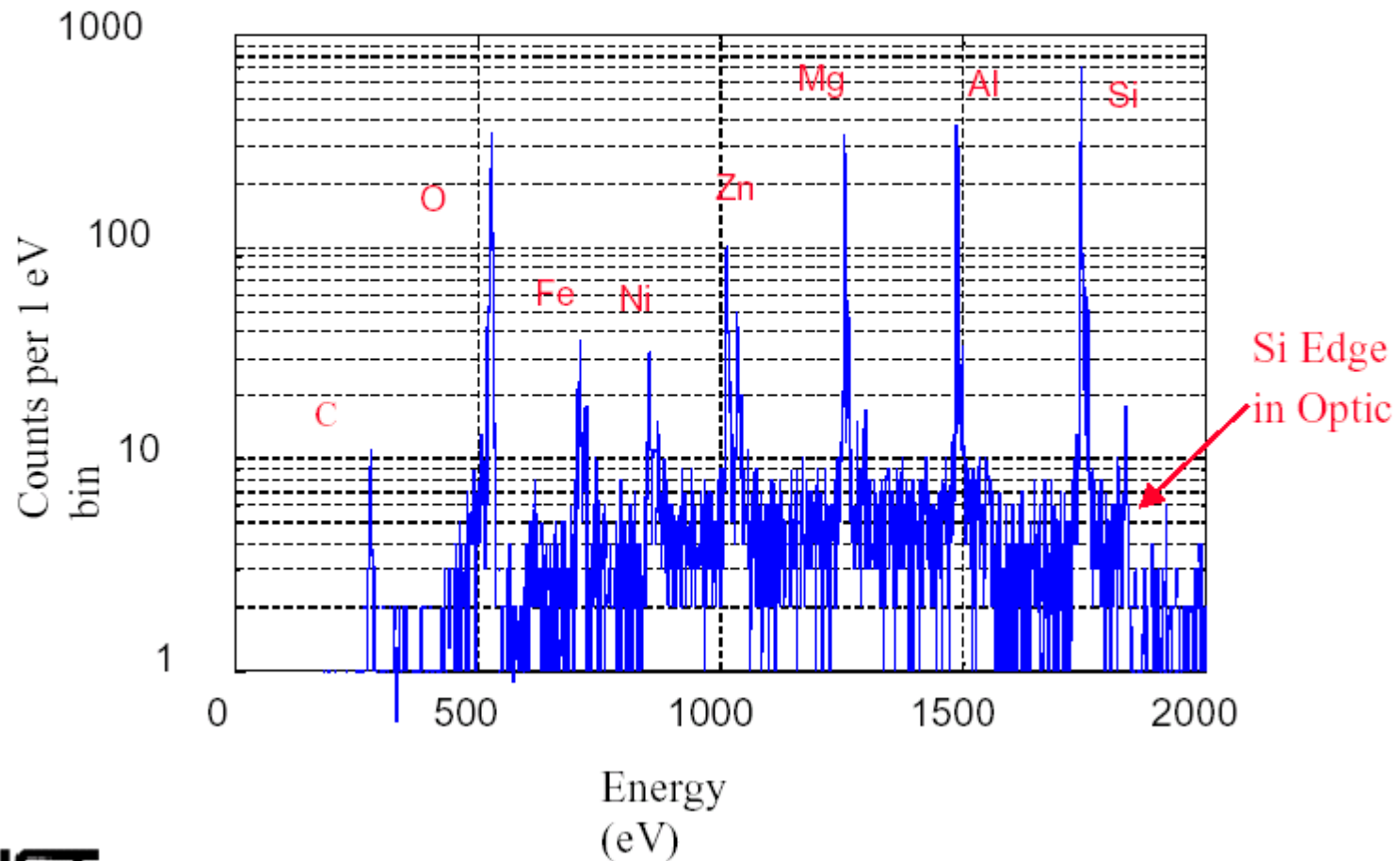
Physical principle

- absorption of a photon
- sudden increase in temperature
- increase in resistivity
- measurement of an electric pulse

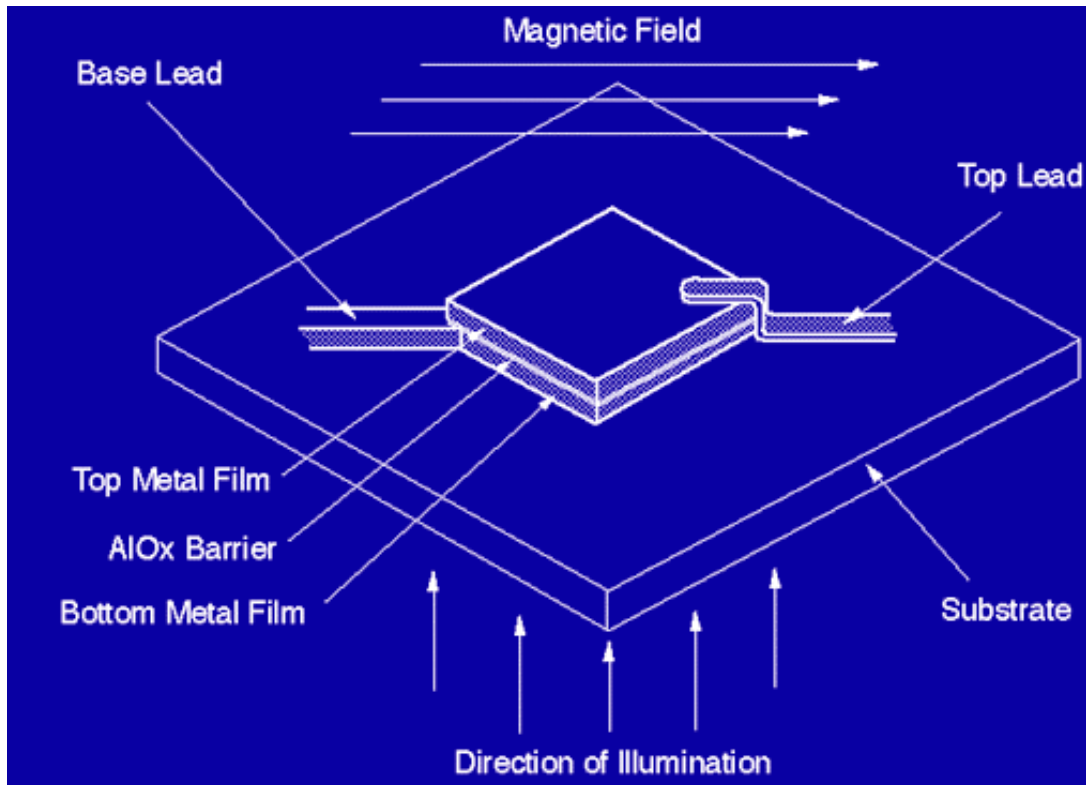


State of the art TES microcalorimeter

Spectrum of NIST glass with Al-Ag TES microcalorimeter



STJ - Superconducting Tunnel Junction (Josephson Junction)



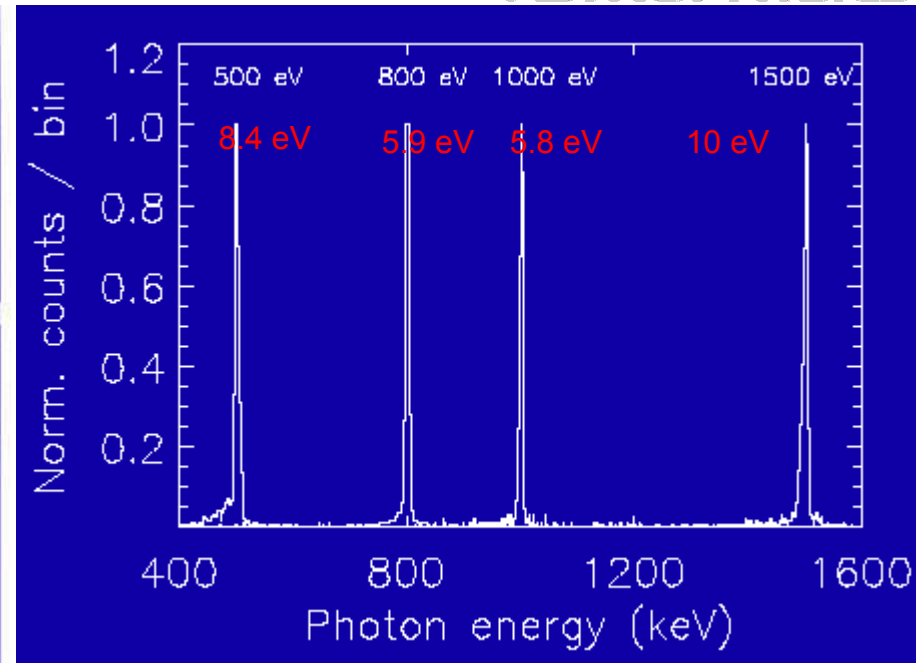
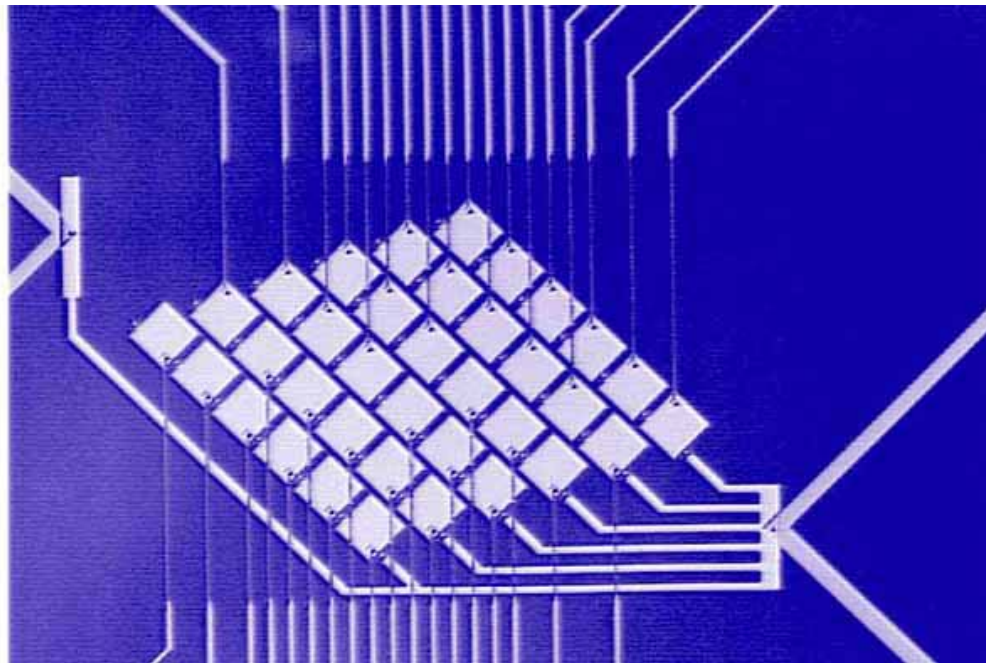
consists of two thin films of a superconducting metal (niobium, tantalum or hafnium) separated by a thin insulating layer

when operated well below the superconductor's critical temperature (below 1 K), the equilibrium state of the junction is easily perturbed by any photon striking it.

The photon is breaking up Cooper pairs (meV binding energy)

by applying a small bias voltage across the junction and a suitable parallel magnetic field to suppress the Josephson current, an electrical charge proportional to the photon energy can be extracted from the device.

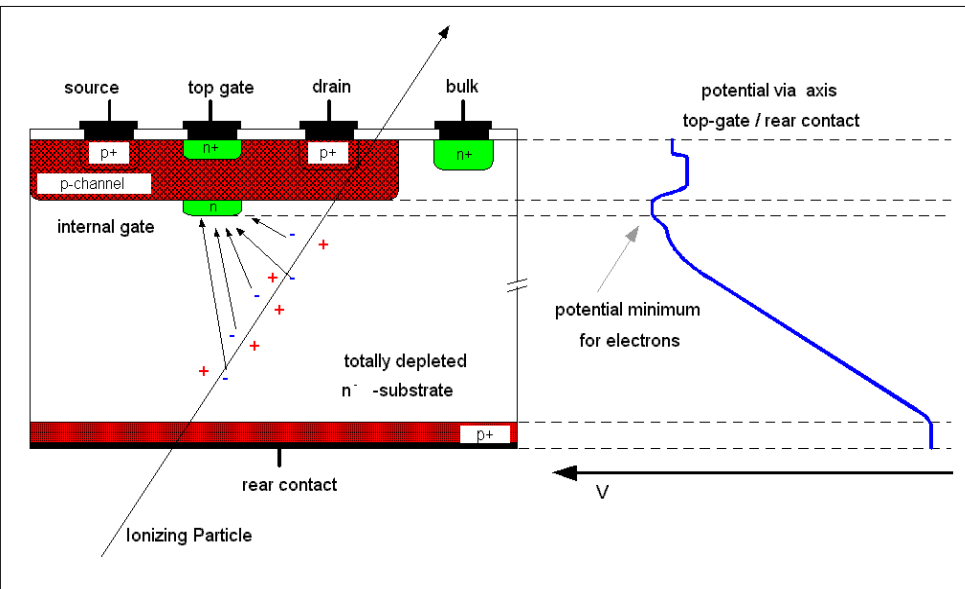
Tantalum STJ Lab Results



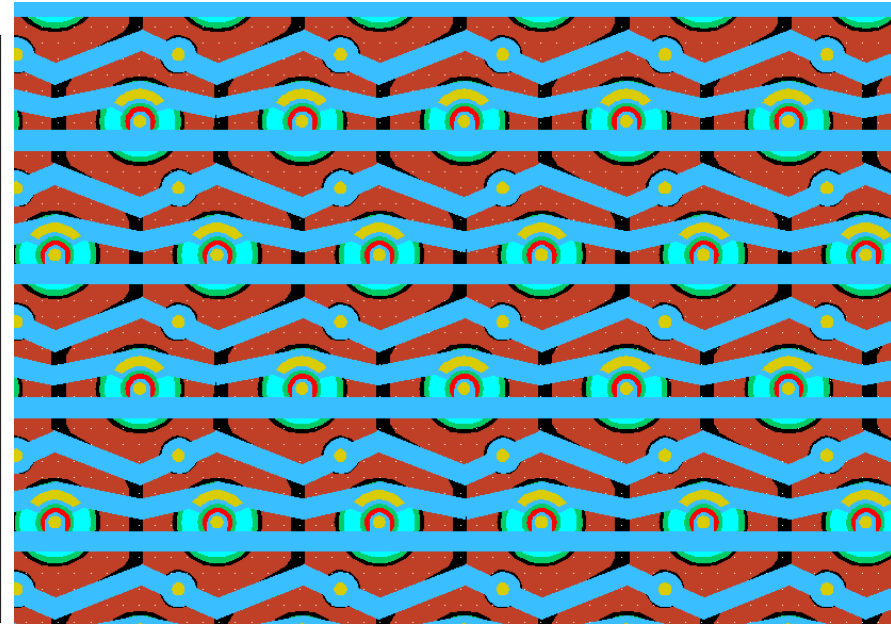
The DEPFET principle

- DEPFET = Fully depleted active field-effect transistor
- a new kind of CCD, where **every pixel** is read-out
 - ➔ very short read-out time

- ring-like shape
- the gate, drain, and source of each of the pixels are visible
- $\sim 10^6$ amplifiers are present



View through one pixel of a DEPFET structure



DEPFET matrix layout

Modern detectors (example XEUS)

Detector	WFI	NFI1	NFI2
Type	DEPFET	STJ	TES/Bolometer
Nr. of Pixels	1000x1000	50x50	32x32
Pixel Size	0.3"	0.6"	1"
FOV	5x5arcmin ²	1x1arcmin ²	1x1arcmin ²
Temperature	200K	350mK	50mK
Resolution	60eV@1keV	1eV@1keV	5eV@8keV

Very high readout rate required because of large throughput !

- WFI = Wide Field Imager
- NFI = Narrow Field Imager
- STJ = Superconducting Tunnel Junction
- TES = Transition Edge Sensor

Spectroscopy Science

